

A Hybrid Delay Model for Interconnected Multi-Input Gates

Arman Ferdowsi, Matthias Függer, Josef Salzmann and Ulrich Schmid
 TU Wien, Embedded Computing Systems Group, Vienna, Austria
 {aferdowsi, jsalzmann, s}@ecs.tuwien.ac.at
 CNRS, LMF, ENS Paris-Saclay, Université Paris-Saclay
 mfuegger@lmf.cnrs.fr

Abstract—Dynamic digital timing analysis is a less accurate but fast alternative to highly accurate but slow analog simulations of digital circuits. It relies on gate delay models, which allow the determination of input-to-output delays of a gate on a per-transition basis. Accurate delay models not only consider the effect of preceding output transitions here but also delay variations induced by multi-input switching (MIS) effects in the case of multi-input gates. Starting out from a first-order hybrid delay model for CMOS two-input NOR gates, we develop a hybrid delay model for Muller C gates and show how to augment these models and their analytic delay formulas by a first-order interconnect. Moreover, we conduct a systematic evaluation of the resulting modeling accuracy: Using SPICE simulations, we quantify the MIS effects on the gate delays under various wire lengths, load capacitances, and input strengths for two different CMOS technologies, comparing these results to the predictions of appropriately parameterized versions of our new gate delay models. Overall, our experimental results reveal that they capture all MIS effects with a surprisingly good accuracy despite being first-order only.

Index Terms—dynamic timing analysis, gate delay models, interconnected multi-input gates, thresholded hybrid systems.

I. INTRODUCTION

Digital timing analysis techniques are indispensable in modern circuit design, as they enable the validation of large designs: Thanks to the elaborate *static timing analysis* techniques available for digital timing analysis nowadays, which employ models like CCSM [1] and ECSM [2] that facilitate an accurate corner case analysis of the delays of the gates making up a digital circuit, worst-case critical path delays can be determined accurately and very fast. Still, corner-case delay estimates have limitations: static timing analysis considers signal transitions in isolation, in the sense that the underlying gate and interconnect delays do not take into account the transition history.

By contrast, *dynamic timing analysis* may uncover a circuit's behavior that becomes only visible when the effect of previous signal transitions is also taken into account. This can be nicely exemplified by means of the token-passing ring described and analyzed by Winstanley et al. in [3]: This asynchronous circuit implements a ring oscillator made up of

stages consisting of a 2-input Muller C gate, the inputs of which are connected to the previous resp. next stage. The authors uncovered that the ring exhibits two modes of operation, namely, burst behavior versus evenly spaced output transitions, which can switch over time. The actual mode depends on the subtle interplay between two effects that determine the delay of a 2-input C gate: the *drafting effect*, a decrease of the delay happening when an output transition is close to the *previous* output transition, and the *Charlie effect*, (named after Charles Molnar, who identified its causes in the 70th of the last century, and nowadays known as a *multiple input switching* (MIS) effect [4]), an increase in the delay happening when the two inputs are switching (in the same direction) in close proximity. Obviously, to analyze the behavior of the ring, the timing relation of *individual* transitions need to be traced throughout the whole circuit.

Analog simulations, e.g., using SPICE [5], are the golden standard for such dynamic timing analyses. Unfortunately, however, analog simulation times are prohibitively excessive even for moderately large circuits, as the dimension of the system of differential equations that need to be solved numerically increases with the number of transistors. By contrast, *digital* dynamic timing analysis techniques rest on *delay models* that provide gate delay estimations on a per-transition basis. Suitable gate delay models allow fast correctness validation and accurate performance and power estimation [6] of a large circuit even at early stages of the development.

The simplest non-trivial¹ digital delay models suitable for accurate dynamic timing analysis are single-history delay models [8], where a gate's input-to-output delay $\delta(T)$ depends solely on the previous-output-to-input delay T . Particularly relevant in this context is the *involution delay model* (IDM) [9], which comprises zero-time gates connected by single-input single-output involution delay channels. IDM channels are characterized by a delay function $\delta(T)$, which is a negative involution $-\delta(-\delta(T)) = T$. Note that the dependence on T captures the drafting effect introduced in [3].

Unlike other known delay models, the IDM faithfully models glitch propagation in the canonical short-pulse filtration problem [8], and even allows to incorporate substantial delay noise as well as PVT variations and aging without compromis-

The research work of Arman Ferdowsi and Josef Salzmann was funded by the Austrian Science Fund (FWF) project DMAC [10.55776/P32431]. Matthias Függer's research was supported by the ANR DREAMY (ANR-21-CE48-0003)

¹The well-known pure and inertial delay models [7] have no or almost no history dependency and are hence considered trivial in our context.

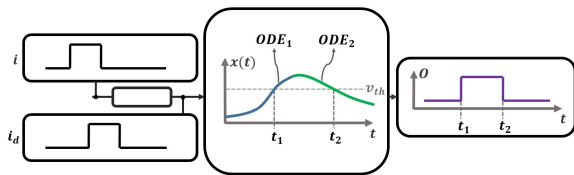


Fig. 1: Illustration of the thresholded hybrid system of an IDM channel, with a single input i and output o . It comprises an (optional) pure delay shifter, producing i_d , and two ODEs governing some state signal $x(t)$ that is digitized by a threshold voltage comparator to produce o . The active ODE is selected by the current state of i_d , with mode switches that guarantee continuity of $x(t)$.

ing faithfulness [10], [11]. A particularly compelling feature of the IDM is its simplicity, which originates in the fact that it can be viewed as a simple 2-state thresholded hybrid model of order 1 [12]. As illustrated in Fig. 1, in such a system, the state of the digital input is used to select one among two *ordinary differential equations* (ODEs) that govern some internal analog signal, the digitized version of which constitutes the digital output. This simplicity allows one to derive explicit analytic formulas for the IDM channel delays $\delta(T)$, which in turn enable very fast digital timing simulation. And indeed, the IDM also comes with a publicly available simulation framework, the *Involution Tool* [13], which also facilitates the evaluation of the accuracy of IDM delay predictions against SPICE-generated data and other delay models. Both measurements [14] and simulations [13] using the Involution Tool showed a very good accuracy for inverter chains and clock trees, albeit less so for circuits containing multi-input gates. In the case of the clock tree, a speedup of a factor of 250 has been obtained relative to SPICE in terms of simulation times here.

In order to further improve the accuracy of digital dynamic timing analysis techniques for multi-input gates, however, gate delay models that explicitly cover MIS effects are inevitable. Models like IDM, which are based on single-input single-output delay channels, are obviously incapable of varying the gate delay based on the time difference Δ between signal transitions at *different* inputs (see Fig. 2 for the MIS delay variations of a real NOR gate). Models capable of capturing MIS effects have of course been addressed in the literature before, with approaches ranging from linear [15] or quadratic [16] fitting over higher-dimensional macromodels [17] and model representations [18] to recent machine learning methods [19]. The resulting models are very complex, however, and definitely way beyond first-order, and thus unsuitable as a basis for fast dynamic digital timing analysis.

In a suite of papers [20]–[22], Ferdowsi et al. developed thresholded hybrid models for 2-input CMOS NOR and NAND gates. These models are all based on replacing transistors by (possibly time-varying) switched resistors. All MIS effects are covered by the model proposed in [21], [22], which is a 4-state hybrid first-order model based on the Shichman-Hodges transistor model [23]. Whereas the ODEs governing its 4 modes are all first-order, they have time-varying coefficients and are hence not trivial to solve analytically. The

delay formulas derived in [21] are hence based on piecewise approximations and thus quite complex. Ultimately, however, explicit solutions for the ODEs were determined and used for deriving simple and accurate analytic delay formulas [22]. Using an explicit parametrization procedure also defined in this paper, the authors showed that appropriately parametrized versions of their model predict the actual delay of NOR gates implemented in different CMOS technologies accurately and fast.

A serious limitation of all the above delay models is that they only consider gates in isolation, however, i.e., without any interconnect. Unfortunately, wires do have a substantial effect on circuit delays in practice: they have non-negligible parasitic capacitances, resistances, and inductances, which are spatially distributed and hence change with the wire length.

The main purpose of this paper² is to explore the delay modeling accuracy achievable with an augmented version of the model of [22], which covers *both* the gate and the interconnect to the successor gate. In addition, to enable dynamic timing analysis of applications such as the token-passing ring [3] mentioned earlier, we also develop a thresholded hybrid delay model for Muller C gates. In order to evaluate the accuracy of our models, we compare their delay predictions to SPICE simulations of different gates with different interconnects. Overall, our experimental results reveal that they capture all MIS effects with a surprisingly good accuracy, despite being first-order only.

Detailed contributions:

- (1) We augment the model from [22] by an RC-type interconnect and determine analytic expressions for the trajectories and the resulting delays. The choice for a simple RC-type model, as opposed to higher-order models, is motivated by the goal of an analytically tractable and simple-to-compute first-order model.
- (2) We extend the parametrization procedure from [22] to also determine the new interconnect-related model parameters. The analytic delay formulas again proved instrumental for developing a sound algorithm here.
- (3) Based on our findings for the NOR gate in (1) and (2), we develop a thresholded hybrid model for the Muller C gate and its parametrization procedure.
- (4) We conduct a series of simulations to determine the accuracy of our augmented models for interconnected NOR and C gates. In our simulations, we consider two different CMOS technologies (15 nm and 65 nm), and vary input driving strength, wire length, load capacitance, wire resistance, and wire capacitance. Using SPICE simulations, we determine $\delta(\Delta)$ for different values of Δ , and compare those to the predictions of an appropriately parametrized version of our gate delay models.

Paper organization: In Section II, we briefly introduce MIS effects in multi-input NOR gates. In Section III, we

²A preliminary version of this paper has appeared at DSD'23 (where it was nominated for the best paper award). This conference version was based on the results of [21], however, which are piecewise approximations of the gate delay. The interconnect extension described in the present paper is based on the explicit delay formulas developed in [22].

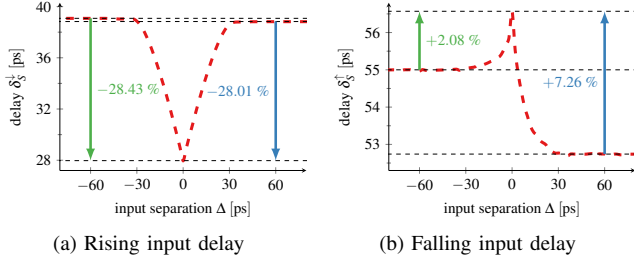


Fig. 2: MIS effects in the measured delay of a 15nm technology CMOS NOR gate. $\Delta = t_B - t_A$ is the input separation time between effective signal transitions at the inputs A and B .

summarize the key points of the thresholded hybrid model for those gates presented in [21], as well as an enhanced version proposed in [22]. In Section IV resp. Section V, we present an interconnect-augmented model, its parametrization, and its experimental accuracy evaluation for NOR resp. C gates. Some conclusions in Section VI round-off our paper.

II. MULTI-INPUT SWITCHING (MIS) EFFECTS

As already mentioned in Section I, the simulation experiments in [13] showed that the prediction accuracy of the simple IDM is below expectations for circuits containing multi-input gates. As revealed by Ferdowsi et al. [20], [21], this is primarily due to the fact that a model of a multi-input gate that combines single-input single-output IDM channels with zero-time Boolean gates cannot properly capture output delay variations caused by *multiple input switching* (MIS) effects: output transitions may be sped up/slowed down when different inputs switch in close temporal proximity [4].

Consider the CMOS implementation of a NOR gate shown in Fig. 3a, which consists of two serial pMOS (T_1 and T_2) for charging the load capacitance C (producing a rising output transition), and two parallel nMOS transistors (T_3 and T_4) for discharging it (producing a falling one). When an input experiences a rising transition, the corresponding nMOS transistor closes while the corresponding pMOS transistor opens, so C will be discharged. If both inputs A and B experience a rising transition at the same time, C is discharged twice as fast. Since the gate delay depends on the discharging speed, it follows that the falling output delay $\delta_S^\downarrow(\Delta)$ increases (by almost 30% in the example shown in Fig. 2a) when the *input separation time* $\Delta = t_B - t_A$ increases from 0 to ∞ or decreases from 0 to $-\infty$. For falling input transitions, the behavior of the NOR gate is quite different: Fig. 2b shows that the MIS effects lead to a moderate decrease of the rising output delay $\delta_S^\uparrow(\Delta)$ when $|\Delta|$ goes from 0 to ∞ , which is primarily caused by capacitive coupling.

III. BACKGROUND: A THRESHOLDED HYBRID MODEL FOR NOR GATES

In this section, we briefly revisit the cornerstones of the advanced thresholded hybrid model for NOR (as well as NAND) gates introduced in [21], [22]. In the following section, we will

TABLE I: State transitions and modes. \uparrow and $\uparrow\uparrow$ (resp. \downarrow and $\downarrow\downarrow$) represent the first and the second rising (resp. falling) input transitions. $+$ and $-$ specify the sign of the switching time difference $\Delta = t_B - t_A$.

Mode	Transition	t_A	t_B	R_1	R_2	R_3	R_4
T_1^\downarrow	(0,0) \rightarrow (1,0)	0	$-\infty$	on \rightarrow off	on	off \rightarrow on	off
$T_1^{\uparrow\uparrow}$	(1,0) \rightarrow (1,1)	$-\Delta$	0	off	on \rightarrow off	on	off \rightarrow on
T_2^\downarrow	(0,0) \rightarrow (0,1)	$-\infty$	0	on	on \rightarrow off	off	off \rightarrow on
$T_2^{\uparrow\uparrow}$	(0,1) \rightarrow (1,1)	0	$-\Delta$	on \rightarrow off	off	off \rightarrow on	on
T_3^\downarrow	(1,1) \rightarrow (0,1)	0	$-\infty$	off \rightarrow on	off	on \rightarrow off	on
$T_3^{\uparrow\uparrow}$	(0,1) \rightarrow (0,0)	$-\Delta$	0	on	off \rightarrow on	off	on \rightarrow off
T_4^\downarrow	(1,1) \rightarrow (1,0)	$-\infty$	0	off	off \rightarrow on	on	on \rightarrow off
$T_4^{\uparrow\uparrow}$	(1,0) \rightarrow (0,0)	0	$-\Delta$	off \rightarrow on	on	on \rightarrow off	off

extend this model to also incorporate the interconnect between gates.

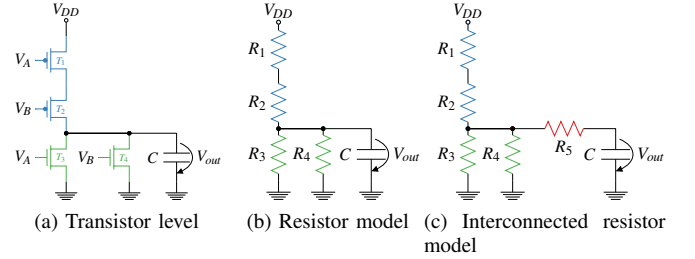


Fig. 3: Transistor schematic and the resistor model of a CMOS NOR gate along with its augmented RC interconnect component.

Rather than representing all transistors by zero-time switches as in [20], the model of a 2-input CMOS NOR gate proposed in [21], [22] replaces (some) transistors in Fig. 3a by time-varying resistors, as shown in Fig. 3b. These resistors, denoted as $R_i(t)$ for $i \in \{1, \dots, 4\}$, vary between a predetermined on-resistance R_i and the off-resistance ∞ . The governing principle for $R_i(t)$, which will be based on the Shichman-Hodges transistor model [23], is contingent upon the state of the corresponding input signal at the gate of the corresponding transistor.

This results in a hybrid model comprising four distinct modes, according to the four possible input states $(A, B) \in \{(0,0), (0,1), (1,0), (1,1)\}$. Table I shows all possible input state transitions and the corresponding resistor time evolution mode switches. Double arrows in the mode switch names indicate MIS-relevant modes, whereas $+$ and $-$ indicate whether input A switched before B or the other way round. For instance, assume the system is in state $(0,0)$ initially, i.e., that both A and B were set to 0 at time $t_A = t_B = -\infty$. This causes R_1 and R_2 to be in the *on-mode*, whereas R_3 and R_4 are in the *off-mode*. If A is switched to 1 at time $t_A = 0$, R_1 resp. R_3 is switched to the off-mode resp. on-mode at time $t_1^{\text{off}} = t_3^{\text{on}} = t_A = 0$. The corresponding mode switch is T_1^{\uparrow} and reaches state $(1,0)$. If B is also switched to 1 at some time $t_B = \Delta > 0$, R_2 resp. R_4 is switched to the off-mode resp. on-mode at time $t_2^{\text{off}} = t_4^{\text{on}} = t_B = \Delta$. The corresponding mode switch is $T_2^{\uparrow\uparrow}$ and reaches state $(1,1)$.

A crucial part of the model is the choice of the governing principle dictating the temporal variation of $R_i(t)$ during the on- and off-mode: It should reasonably model the actual be-

havior of a transistor while facilitating the analytical solvability of the ensuing ordinary differential equation (ODE) systems. In [21], the continuous resistance model defined by

$$R_j^{on}(t) = \frac{\alpha_j}{t - t^{on}} + R_j; \quad t \geq t^{on}, \quad (1)$$

$$R_j^{off}(t) = \beta_j(t - t^{off}) + R_j; \quad t \geq t^{off}, \quad (2)$$

for some constant slope parameters α_j [Ω s], β_j [Ω /s], and on-resistance R_j [Ω] is used; t^{on} resp. t^{off} represent the time when the respective transistor is switched on resp. off. These equations are based on the Shichman-Hodges transistor model [23], which assumes a quadratic correlation between the output current and the input voltage: Eq. (1) and Eq. (2) follow from approximating the latter by $d\sqrt{t - t_0}$ in the operation range close to the threshold voltage V_{th} , with d and t_0 denoting appropriate fitting parameters.

Interestingly, continuously varying resistors are only needed for switching on the pMOS transistors in [21]. In addition, rather than including $R_1(t)$ and $R_2(t)$ in the state of the ODEs governing the appropriate modes, which would blow-up their dimensions, they are incorporated by means of time-varying coefficients in simple first-order ODEs. All other transistor switchings, i.e., both the switching-off of the pMOS transistors and any switching on or off of the nMOS transistors, happen instantaneously, as already employed in [20], which is accomplished by choosing the model parameters $\alpha_i = 0$ in Eq. (1) for $i \in \{3, 4\}$, and $\beta_k = \infty$ in Eq. (2) for $k \in \{1, \dots, 4\}$.

In what follows, we will use the notation $R_1 = R_{pA}$, $R_2 = R_{pB}$ with the abbreviation $2R = R_{pA} + R_{pB}$ for the two pMOS transistors T_1 and T_2 and $R_3 = R_{nA}$, $R_4 = R_{nB}$ for the two nMOS transistors T_3 and T_4 . Applying Kirchhoff's rules to Fig. 3b results in the the non-autonomous, non-homogeneous ODE with non-constant coefficients

$$\frac{dV_{out}}{dt} = -\frac{V_{out}}{C R_g(t)} + U(t), \quad (3)$$

where $\frac{1}{R_g(t)} = \frac{1}{R_1(t) + R_2(t)} + \frac{1}{R_3(t)} + \frac{1}{R_4(t)}$ and $U(t) = \frac{V_{DD}}{C(R_1(t) + R_2(t))}$. It is well-known that the general solution of (3) is

$$V_{out}(t) = V_0 e^{-G(t)} + \int_0^t U(s) e^{G(s) - G(t)} ds, \quad (4)$$

where $V_0 = V_{out}(0)$ denotes the initial condition and $G(t) = \int_0^t (C R_g(s))^{-1} ds$. As comprehensively described in [21], depending on each particular resistor's mode in each input state transition, different expressions for $R_g(t)$ and $U(t)$ are obtained. Denoting $I_1 = \int_0^t \frac{ds}{R_1(s) + R_2(s)}$, $I_2 = \int_0^t \frac{ds}{R_3(s)}$, and $I_3 = \int_0^t \frac{ds}{R_4(s)}$, Table II summarizes those. The following Theorem 1 provides the resulting analytic formulas.

Theorem 1 (Output voltage trajectories for the NOR gate [22, Theorems 6.2 and 6.3]). *For any $0 \leq |\Delta| \leq \infty$, the*

TABLE II: Integrals $I_1(t)$, $I_2(t)$, $I_3(t)$ and the function $U(t)$ for every possible mode switch; $\Delta = t_B - t_A$, and $2R = R_{pA} + R_{pB}$.

Mode	$I_1(t) = \int_0^t \frac{ds}{R_1(s) + R_2(s)}$	$I_2(t) = \int_0^t \frac{ds}{R_3(s)}$	$I_3(t) = \int_0^t \frac{ds}{R_4(s)}$	$U(t) = \frac{V_{DD}}{C(R_1(t) + R_2(t))}$
T_1^\downarrow	$\int_0^t (1/R_{nA}) ds$	0	0	0
T_1^\uparrow	0	$\int_0^t (1/R_{nA}) ds$	$\int_0^t (1/R_{nB}) ds$	0
T_2^\downarrow	0	0	$\int_0^t (1/R_{nB}) ds$	0
T_2^\uparrow	0	$\int_0^t (1/R_{nA}) ds$	$\int_0^t (1/R_{nB}) ds$	0
T_3^\downarrow	0	0	$\int_0^t (1/R_{nB}) ds$	0
T_3^\uparrow	$\int_0^t (1/(\frac{\alpha_1}{s+\Delta} + \frac{\alpha_2}{s} + 2R)) ds$	0	0	$\frac{V_{DD}(t+\Delta)}{C(2R^2 + (\alpha_1 + \alpha_2 + 2R)t + \alpha_2\Delta)}$
T_4^\downarrow	0	$\int_0^t (1/R_{nA}) ds$	0	0
T_4^\uparrow	$\int_0^t (1/(\frac{\alpha_1}{s} + \frac{\alpha_2}{s+ \Delta } + 2R)) ds$	0	0	$\frac{V_{DD}(t+ \Delta)}{C(2R^2 + (\alpha_1 + \alpha_2 + 2 \Delta)t + \alpha_1 \Delta)}$

output voltage trajectory functions of our model for rising input transitions are given by

$$V_{out}^{T_1^\uparrow}(t) = V_{out}^{T_1^\uparrow}(0) e^{-\frac{t}{C R_{nA}}}, \quad (5)$$

$$V_{out}^{T_2^\uparrow}(t) = V_{out}^{T_2^\uparrow}(0) e^{-\frac{t}{C R_{nB}}}, \quad (6)$$

$$V_{out}^{T_3^\uparrow}(t) = V_{out}^{T_3^\uparrow}(\Delta) e^{-\left(\frac{1}{C R_{nA}} + \frac{1}{C R_{nB}}\right)t}, \quad (7)$$

$$V_{out}^{T_4^\uparrow}(t) = V_{out}^{T_4^\uparrow}(\Delta) e^{-\left(\frac{1}{C R_{nA}} + \frac{1}{C R_{nB}}\right)t}. \quad (8)$$

The output voltage trajectory functions for falling input transitions are given by

$$V_{out}^{T_1^\downarrow}(t) = V_{out}^{T_1^\downarrow}(0) e^{-\frac{t}{C R_{nB}}}, \quad (9)$$

$$V_{out}^{T_2^\downarrow}(t) = V_{out}^{T_2^\downarrow}(0) e^{-\frac{t}{C R_{nA}}}, \quad (10)$$

$$V_{out}^{T_3^\downarrow}(t) = V_{DD} + (V_{out}^{T_3^\downarrow}(\Delta) - V_{DD}) \cdot \left[e^{-\frac{t}{2RC}} \left(1 + \frac{2t}{d + \sqrt{\chi}}\right)^{\frac{-A+a}{2RC}} \left(1 + \frac{2t}{d - \sqrt{\chi}}\right)^{\frac{A}{2RC}} \right], \quad (11)$$

where $a = \frac{\alpha_1 + \alpha_2}{2R}$, $d = a + \Delta$, $\chi = d^2 - 4c'$, $c' = \frac{\alpha_2\Delta}{2R}$, and $A = \frac{\alpha_2\Delta - aR(d - \sqrt{\chi})}{2R\sqrt{\chi}}$. The output voltage trajectory $V_{out}^{T_3^\downarrow}(t)$ for negative Δ is obtained from Eq. (11) by exchanging α_1 and α_2 , $V_{out}^{T_3^\downarrow}(\Delta)$ by $V_{out}^{T_3^\downarrow}(|\Delta|)$, and Δ by $|\Delta|$ in d , χ and A .

The trajectories $V_{out}^{T_1^\uparrow}(t)$, $V_{out}^{T_2^\uparrow}(t)$ and $V_{out}^{T_3^\downarrow}(t)$, $V_{out}^{T_4^\downarrow}(t)$ in Theorem 1 are specifically tailored to facilitate the computation of the MIS delays. For example, the formulas Eq. (7) and Eq. (11) (for $\Delta \geq 0$) have been determined according to the following two procedures:

- (i) Compute $V_{out}^{T_1^\uparrow}(\Delta)$ for the first transition $(0, 0) \rightarrow (1, 0)$ and use it as the initial value for $V_{out}^{T_2^\uparrow}(t)$ governing the second transition $(1, 0) \rightarrow (1, 1)$; the ultimately sought MIS delay $\delta_{M,+}^\uparrow(\Delta)$ is the time (measured from the first transition until either the first or the second trajectory crosses the threshold voltage $V_{DD}/2$ from above when the first one starts from $V_{out}^{T_1^\uparrow}(0) = V_{DD}$).
- (ii) Compute $V_{out}^{T_2^\downarrow}(\Delta)$ for the first transition $(1, 1) \rightarrow (0, 1)$ and use it as the initial value for $V_{out}^{T_3^\downarrow}(t)$ governing the second transition $(0, 1) \rightarrow (0, 0)$; the ultimately sought MIS delay $\delta_{M,+}^\downarrow(\Delta)$ is the time (measured from the second transition) until the second trajectory crosses the threshold voltage $V_{DD}/2$ from below when the first one starts from $V_{out}^{T_2^\downarrow}(0) = 0$.

Clearly, actually determining these MIS delays requires inverting the appropriate trajectory formulas, which turned out

to be easy in the rising input transition case (i) but difficult in the falling input transition case (ii). In [21], a somewhat complicated piecewise approximation (in terms of Δ) of both the trajectory and, hence, the corresponding delay formula was used (these approximations also formed the basis for the preliminary version [24] of the present paper). In [22], however, an explicit trajectory formula was found also for the falling input transition case. According to Eq. (11), $\delta_{M,+}^{\uparrow}(\Delta)$ is the solution (in t) of the implicit function $I(t, \Delta) = 0$, where

$$I(t, \Delta) = e^{\frac{-t}{2RC}} \left(1 + \frac{2t}{d + \sqrt{\chi}}\right)^{\frac{-A+a}{2RC}} \left(1 + \frac{2t}{d - \sqrt{\chi}}\right)^{\frac{A}{2RC}} - \frac{1}{2}. \quad (12)$$

Unfortunately, since $\lim_{\Delta \rightarrow 0} A = 0$ and $\lim_{\Delta \rightarrow 0} (d - \sqrt{\chi}) = 0$, the point $(t, \Delta) = (0, 0)$ is singular for $I(t, \Delta) = 0$, so solving the latter for $t = \delta(\Delta)$ by means of the implicit function theorem is impossible. However, the bootstrapping method [25] was successfully employed for developing an accurate asymptotic expansion of $\delta(\Delta)$ for $\Delta \rightarrow 0$. Theorem 2 provide the resulting MIS delay formulas for an isolated two-input NOR gate, for both rising and falling input transitions as well as positive and negative Δ .

Theorem 2 (MIS delay functions for the NOR gate [22, Theorems 6.4 and 6.5]). *For any $0 \leq |\Delta| \leq \infty$, the MIS delay functions of our model for the rising and falling input transitions are respectively given by*

$$\delta_{M,+}^{\downarrow}(\Delta) = \begin{cases} \frac{\log(2)CRn_A Rn_B - \Delta Rn_B}{Rn_A + Rn_B} + \Delta & 0 \leq \Delta < \log(2)CRn_A \\ \log(2)CRn_A & \Delta \geq \log(2)CRn_A \end{cases} \quad (13)$$

$$\delta_{M,-}^{\downarrow}(\Delta) = \begin{cases} \frac{\log(2)CRn_A Rn_B + |\Delta| Rn_A}{Rn_A + Rn_B} + |\Delta| & |\Delta| < \log(2)CRn_B \\ \log(2)CRn_B & |\Delta| \geq \log(2)CRn_B \end{cases} \quad (14)$$

$$\delta_{M,+}^{\uparrow}(\Delta) = \begin{cases} \delta_0 - \frac{\alpha_1}{\alpha_1 + \alpha_2} \Delta & 0 \leq \Delta < \frac{(\alpha_1 + \alpha_2)(\delta_0 - \delta_{-\infty})}{\alpha_1} \\ \delta_{-\infty} & \Delta \geq \frac{(\alpha_1 + \alpha_2)(\delta_0 - \delta_{-\infty})}{\alpha_1} \end{cases} \quad (15)$$

$$\delta_{M,-}^{\uparrow}(\Delta) = \begin{cases} \delta_0 - \frac{\alpha_2}{\alpha_1 + \alpha_2} |\Delta| & 0 \leq |\Delta| < \frac{(\alpha_1 + \alpha_2)(\delta_0 - \delta_{-\infty})}{\alpha_2} \\ \delta_{-\infty} & |\Delta| \geq \frac{(\alpha_1 + \alpha_2)(\delta_0 - \delta_{-\infty})}{\alpha_2} \end{cases} \quad (16)$$

where

$$\delta_0 = -\frac{\alpha_1 + \alpha_2}{2R} \left[1 + W_{-1} \left(\frac{-1}{e \cdot 2^{\frac{4R^2 C}{\alpha_1 + \alpha_2}}} \right) \right], \quad (17)$$

$$\delta_{-\infty} = -\frac{\alpha_2}{2R} \left[1 + W_{-1} \left(\frac{-1}{e \cdot 2^{\frac{4R^2 C}{\alpha_2}}} \right) \right], \quad (18)$$

$$\delta_{-\infty} = -\frac{\alpha_1}{2R} \left[1 + W_{-1} \left(\frac{-1}{e \cdot 2^{\frac{4R^2 C}{\alpha_1}}} \right) \right]. \quad (19)$$

Herein, $y = W_{-1}(x)$ is the non-principal real branch of the Lambert W function (that solves $ye^y = x$ for $y \leq -1$).

IV. AN ACCURATE HYBRID MIS DELAY MODEL FOR INTERCONNECTED NOR GATES

In this section, we will extend the thresholded hybrid model for an isolated NOR gate surveyed in Section III by adding a simple interconnect. State-of-the-art interconnect modeling usually breaks up wires into segments, each of which is

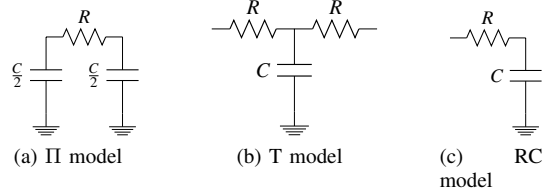


Fig. 4: Lumped models for wires.

characterized by some lumped model, typically of Π , T, and RC type [26], as depicted in Fig. 4.

Since our focus is on exploring the modeling accuracy achievable with first-order hybrid models, we restrict our attention to the lumped RC model, as shown in Fig. 4c: Although this model is known to be less accurate than e.g. the Π model in static timing analysis, it is the only one that can be added to the gate model of [21] without considerably increasing the complexity and turning it into a second-order model: Adding a Π model would add another state-holding stage (capacitor) and hence raise the dimension of the ODE systems to 2.

A. Model extension

Integrating Fig. 4c into the NOR gate results in the schematics shown in Fig. 3c. By applying Kirchoff's rules, the non-homogeneous ODE

$$\frac{dV_{out}(t)}{dt} = -\frac{V_{out}(t)}{C R_g(t) \left(\frac{R_5}{R_g(t)} + 1 \right)} + \frac{V_{DD}}{C(R_1(t) + R_2(t)) \left(\frac{R_5}{R_g(t)} + 1 \right)}, \quad (20)$$

is easily derived. Note that Eq. (20) is just Eq. (3) with the additional factor $f(t) = 1 / \left(\frac{R_5}{R_g(t)} + 1 \right)$ in all terms except $\frac{dV_{out}(t)}{dt}$. Since this non-constant factor $f(t)$ makes solving this ODE explicitly very hard, if at all possible, we decided to take the “easy route” of approximating $f(t)$ by a constant value F : This allows us to re-use the solutions obtained for Eq. (3), by just replacing C with $\frac{C}{F}$ in all output voltage trajectory formulas. In order to reduce the approximation error, however, we use different values of F in different modes.

Recall that in the original hybrid model, each mode switch enables some specific ODE system, the solution of which gives the respective trajectory. Fortunately, as can be observed in Table I, all transitions except $(0, 1) \rightarrow (0, 0)$ and $(1, 0) \rightarrow (0, 0)$ lead to a constant value for $R_g(t)$ and hence F a priori. Consequently, for those six transitions, we can safely substitute $f(t)$ by the appropriate constant value.

Unfortunately, this is not the case for the transitions $(0, 1) \rightarrow (0, 0)$ and $(1, 0) \rightarrow (0, 0)$, though, so replacing $f(t)$ by some constant value introduces some approximation error. Fortunately, the time span during which $R_g(t)$ varies significantly here is very small. Moreover, its variability is not very large either: In particular, as the switch-on of a transistor is fast, one may reasonably conjecture that replacing $f(t)$ by $1 / \left(\frac{R_5}{R_{g_{min}}} + 1 \right)$ should lead to a good approximation; and indeed, the results of our validation experiments in Section IV-C

TABLE III: Input mode switching and the resulting values for $R_g(t)$ and the corresponding approximation F for $f(t)$.

MS	$R_g(t)$	F
$(0, 0) \rightarrow (1, 0)$ and $(1, 1) \rightarrow (1, 0)$	$= R_{n_A}$	$= \frac{R_{n_A}}{R_5 + R_{n_A}}$
$(1, 0) \rightarrow (1, 1)$ and $(0, 1) \rightarrow (1, 1)$	$= \frac{R_{n_A} R_{n_B}}{R_{n_A} + R_{n_B}}$	$= \frac{R_{n_A} R_{n_B}}{R_5(R_{n_A} + R_{n_B}) + R_{n_A} R_{n_B}}$
$(0, 0) \rightarrow (0, 1)$ and $(1, 1) \rightarrow (0, 1)$	$= R_{n_B}$	$= \frac{R_{n_B}}{R_5 + R_{n_B}}$
$(0, 1) \rightarrow (0, 0)$ and $(1, 0) \rightarrow (0, 0)$	$\approx 2R$	$\approx \frac{2R}{R_5 + 2R}$

will confirm this conjecture. That $1/R_{g_{min}} = 1/(2R)$ follows from Table I, which reveals that $(0, 1) \rightarrow (0, 0)$ resp. $(1, 0) \rightarrow (0, 0)$ leads to $1/R_g(t) = 1/(\frac{\alpha_1}{t+\Delta} + \frac{\alpha_2}{t} + 2R)$ resp. $= 1/(\frac{\alpha_1}{t} + \frac{\alpha_2}{t+\Delta} + 2R)$.

Table III summarizes all exact and approximate values of $R_g(t)$ and F corresponding to each mode switch.

The results of the above discussion are summarized in the following Corollary 1, which gives the delay predictions of our interconnect-augmented model. It is identical to Theorem 2, except that C is replaced by C/F for the appropriate transitions (recall the procedure (i) and (ii) in Section III), where F is given in Table III.

Corollary 1 (MIS delay functions for the interconnect-augmented NOR gate). *For any $0 \leq |\Delta| \leq \infty$, the MIS delay functions of our interconnect-augmented model for rising and falling input transitions are respectively given by*

$$\delta_{M,+}^{\downarrow}(\Delta) = \begin{cases} \frac{\log(2)C_2 R_{n_A} R_{n_B} - \frac{C_2 \Delta R_{n_B}}{C_1} + \Delta}{R_{n_A} + R_{n_B}} & 0 \leq \Delta < \log(2)C_1 R_{n_A} \\ \log(2)C_1 R_{n_A} & \Delta \geq \log(2)C_1 R_{n_A} \end{cases} \quad (21)$$

$$\delta_{M,-}^{\downarrow}(\Delta) = \begin{cases} \frac{\log(2)C_2 R_{n_A} R_{n_B} + \frac{C_2}{C_1} |\Delta| R_{n_A}}{R_{n_A} + R_{n_B}} + |\Delta| & |\Delta| < \log(2)C_1' R_{n_B} \\ \log(2)C_1' R_{n_B} & |\Delta| \geq \log(2)C_1' R_{n_B} \end{cases} \quad (22)$$

$$\delta_{M,+}^{\uparrow}(\Delta) = \begin{cases} \delta_0 - \frac{\alpha_1}{\alpha_1 + \alpha_2} \Delta & 0 \leq \Delta < \frac{(\alpha_1 + \alpha_2)(\delta_0 - \delta_{-\infty})}{\alpha_1} \\ \delta_{-\infty} & \Delta \geq \frac{(\alpha_1 + \alpha_2)(\delta_0 - \delta_{-\infty})}{\alpha_1} \end{cases} \quad (23)$$

$$\delta_{M,-}^{\uparrow}(\Delta) = \begin{cases} \delta_0 - \frac{\alpha_2}{\alpha_1 + \alpha_2} |\Delta| & 0 \leq |\Delta| < \frac{(\alpha_1 + \alpha_2)(\delta_0 - \delta_{-\infty})}{\alpha_2} \\ \delta_{-\infty} & |\Delta| \geq \frac{(\alpha_1 + \alpha_2)(\delta_0 - \delta_{-\infty})}{\alpha_2} \end{cases} \quad (24)$$

where

$$\delta_0 = -\frac{\alpha_1 + \alpha_2}{2R} \left[1 + W_{-1} \left(\frac{-1}{e \cdot 2^{\frac{4R^2 C_3}{\alpha_1 + \alpha_2}}} \right) \right], \quad (25)$$

$$\delta_{\infty} = -\frac{\alpha_2}{2R} \left[1 + W_{-1} \left(\frac{-1}{e \cdot 2^{\frac{4R^2 C_3}{\alpha_2}}} \right) \right], \quad (26)$$

$$\delta_{-\infty} = -\frac{\alpha_1}{2R} \left[1 + W_{-1} \left(\frac{-1}{e \cdot 2^{\frac{4R^2 C_3}{\alpha_1}}} \right) \right], \quad (27)$$

$$C_1 = \frac{C(R_5 + R_{n_A})}{R_{n_A}}, \quad (28)$$

$$C_1' = \frac{C(R_5 + R_{n_B})}{R_{n_B}}, \quad (29)$$

$$C_2 = \frac{C(R_5(R_{n_A} + R_{n_B}) + R_{n_A} R_{n_B})}{R_{n_A} R_{n_B}}, \quad (30)$$

$$C_3 = \frac{C(R_5 + 2R)}{2R}. \quad (31)$$

Proof. We give the proof for $\delta_{M,+}^{\downarrow}(\Delta)$ only; the expression for $\delta_{M,-}^{\downarrow}(\Delta)$ can be derived from the former by exchanging R_{n_A}

and R_{n_B} and replacing Δ by $|\Delta|$. First, consider the transition $(1, 0) \rightarrow (1, 1)$ and the corresponding trajectory $V_{out}^{T^{\uparrow\uparrow}}(t)$ in procedure (i) stated after Theorem 1. According to Table III, it is just Eq. (7) with C replaced by C_2 here, i.e.,

$$V_{out}^{T^{\uparrow\uparrow}}(t) = V_{out}^{T^{\uparrow}}(\Delta) e^{-\left(\frac{1}{C_2 R_{n_A}} + \frac{1}{C_2 R_{n_B}}\right)t}. \quad (32)$$

This trajectory must start from the initial value

$$V_{out}^{T^{\uparrow}}(\Delta) = V_{out}^{T^{\uparrow}}(0) e^{\frac{-\Delta}{C_1 R_{n_A}}}, \quad (33)$$

associated with the transition $(0, 0) \rightarrow (1, 0)$, which results from replacing C by C_1 in Eq. (5). The latter, in turn, starts from $V_{out}^{T^{\uparrow}}(0) = V_{DD}$. The goal is to determine the time $\delta_{M,+}^{\downarrow}(\Delta)$ when $V_{DD}/2$ is reached from above either by (a) the first trajectory $V_{out}^{T^{\uparrow}}(t)$ if Δ is large, or (b) by $V_{out}^{T^{\uparrow\uparrow}}(t)$ itself (which commences at time Δ , i.e., $t = 0$ corresponds to Δ here) if Δ is small enough. Given that both trajectories involve only a single exponential function, they are straightforward to invert. From Eq. (33), it is evident that case (a) occurs for $\Delta \geq \log(2)C_1 R_{n_A}$, while Eq. (32) governs case (b) for smaller values of Δ . It is not hard to confirm that this gives raise to Eq. (21), which differs from Eq. (13) only in that ΔR_{n_B} in the numerator for case (b) has been replaced by $\frac{C_2}{C_1} \Delta R_{n_B}$.

Obtaining $\delta_{M,+}^{\uparrow}(\Delta)$ is even simpler, since $V_{out}^{T^{\downarrow}}(\Delta) = 0$ in procedure (ii), as it starts from $V_{out}^{T^{\downarrow}}(0) = 0$ and follows Eq. (9). Consequently, only $V_{out}^{T^{\downarrow\downarrow}}(t)$ starting from initial value 0 is relevant here. All that is needed is hence to replace C by C_3 in Eq. (11). Consequently, the MIS delay formula Eq. (15) remains valid, provided C is replaced by C_3 in Eq. (17)-Eq. (19). This justifies Eq. (23) and Eq. (25)-Eq. (27). The MIS delay formula Eq. (24) for negative Δ follows from exchanging α_1 and α_2 and replacing Δ by $|\Delta|$ in Eq. (23). \square

B. Model parametrization

For the applicability of Corollary 1, it is essential to have a practical procedure for model parameterization: Given the *extremal* MIS delay values of a real interconnected NOR gates, namely $\delta_S^{\downarrow}(-\infty)$, $\delta_S^{\downarrow}(0)$, and $\delta_S^{\downarrow}(\infty)$ according to Fig. 2a, and $\delta_S^{\uparrow}(-\infty)$, $\delta_S^{\uparrow}(0)$, and $\delta_S^{\uparrow}(\infty)$ according to Fig. 2b, we want to determine suitable values for the parameters α_1 , α_2 , C , R , R_{n_A} , R_{n_B} , and R_5 such that the MIS delays predicted by our model *match* these values, in the sense that $\delta_{M,-}^{\downarrow}(-\infty) = \delta_S^{\downarrow}(-\infty)$, $\delta_{M,-}^{\downarrow}(0) = \delta_{M,+}^{\downarrow}(0) = \delta_S^{\downarrow}(0)$, $\delta_{M,+}^{\downarrow}(\infty) = \delta_S^{\downarrow}(\infty)$ and $\delta_{M,-}^{\uparrow}(-\infty) = \delta_S^{\uparrow}(-\infty)$, $\delta_{M,-}^{\uparrow}(0) = \delta_{M,+}^{\uparrow}(0) = \delta_S^{\uparrow}(0)$, $\delta_{M,+}^{\uparrow}(\infty) = \delta_S^{\uparrow}(\infty)$.

For the isolated NOR gate model proposed in [21], matching parameter values could only be determined after adding some well-chosen minimal pure delay $\delta_{min} > 0$ to the model. Note carefully that adding such a non-zero minimal pure delay to the model is also mandatory for making it *causal*, see [12], [22] for details. Thanks to the explicit delay formulas developed in [22], given in Theorem 2, the least-squares fitting-based parametrization procedure used in [21] could be replaced by explicit formulas for computing the sought parameters. These

formulas also allowed to compute the required value for δ_{\min} , see [22, Thm. 6.6].

Since we cannot re-use these analytic parametrization formulas for our interconnect-augmented model directly, due to the additional parameter R_5 , Theorem 3 provides a suitably adapted parameterization procedure. Interestingly, the additional degree of freedom provided by R_5 removed the need for a uniquely determined value of δ_{\min} . Indeed, it turned out that the new parametrization procedure works for almost any reasonable choice of δ_{\min} , in the sense that delay predictions provided by the appropriately parametrized model are the same. To determine the particular values of δ_{\min} for the parametrizations in Section IV-C, we just used the procedure for measuring the pure delay for inverters proposed by Maier et al. in [27], by tying together inputs A and B of our NOR gates.

Theorem 3 (Model parametrization for interconnect-augmented NOR gates). *Let $\delta_{\min} > 0$ be the pure delay and $\delta_S^\downarrow(-\infty)$, $\delta_S^\downarrow(0)$, $\delta_S^\downarrow(\infty)$ and $\delta_S^\uparrow(-\infty)$, $\delta_S^\uparrow(0)$, $\delta_S^\uparrow(\infty)$ be the MIS delay values of a real interconnected NOR gate that shall be matched by our model. Given an arbitrary chosen value C for the load capacitance, this is accomplished by choosing the model parameters as follows:*

$$R_5 = \frac{(\delta_S^\downarrow(0) - \delta_{\min} - \epsilon)}{\log(2)C} \quad (34)$$

$$R_{n_A} = \frac{\delta_S^\downarrow(\infty) - \delta_S^\downarrow(0) + \epsilon}{\log(2)C} \quad (35)$$

$$R_{n_B} = \frac{\delta_S^\downarrow(-\infty) - \delta_S^\downarrow(0) + \epsilon}{\log(2)C} \quad (36)$$

$$\epsilon = \sqrt{(\delta_S^\downarrow(\infty) - \delta_S^\downarrow(0))(\delta_S^\downarrow(-\infty) - \delta_S^\downarrow(0))} \quad (37)$$

Furthermore, using the function

$$A(t, R, R_5, C) = \frac{-2R(t - C(R_5 + 2R) \cdot \log(2))}{W_{-1}\left(\left(\frac{C(R_5 + 2R) \cdot \log(2)}{t} - 1\right)e^{\frac{C(R_5 + 2R) \cdot \log(2)}{t} - 1}\right) + 1 - \frac{C(R_5 + 2R) \cdot \log(2)}{t}}, \quad (38)$$

determine R by numerically³ solving the equation

$$A(\delta_S^\uparrow(0) - \delta_{\min}, R, R_5, C) - A(\delta_S^\uparrow(\infty) - \delta_{\min}, R, C) - A(\delta_S^\uparrow(-\infty) - \delta_{\min}, R, C) = 0, \quad (39)$$

and finally choose

$$\alpha_1 = A(\delta_S^\uparrow(-\infty) - \delta_{\min}, R, R_5, C), \quad (40)$$

$$\alpha_2 = A(\delta_S^\uparrow(\infty) - \delta_{\min}, R, R_5, C). \quad (41)$$

Proof. The proof follows the general strategy of the proof of [22, Thm. 6.6]. We first consider the parameters determined by the rising input transition case. To align the delay formulas in Corollary 1 with the given extremal delay values, we just plug in $\delta_S^\downarrow(-\infty) - \delta_{\min}$, $\delta_S^\downarrow(0) - \delta_{\min}$, and $\delta_S^\downarrow(\infty) - \delta_{\min}$ to obtain

the following system of equations for our sought parameters δ_{\min} , R_{n_A} , R_{n_B} , and R_5 :

$$\delta_S^\downarrow(0) - \delta_{\min} - \frac{\log(2) \cdot C_2 \cdot R_{n_A} R_{n_B}}{R_{n_A} + R_{n_B}} = 0 \quad (42)$$

$$\delta_S^\downarrow(\infty) - \delta_{\min} - \log(2) \cdot C_1 \cdot R_{n_A} = 0 \quad (43)$$

$$\delta_S^\downarrow(-\infty) - \delta_{\min} - \log(2) \cdot C_1' \cdot R_{n_B} = 0 \quad (44)$$

Plugging Eq. (30) into Eq. (42) gives:

$$\delta_S^\downarrow(0) - \delta_{\min} = \frac{\log(2) \cdot C[R_5(R_{n_A} + R_{n_B}) + R_{n_A}R_{n_B}]}{R_{n_A} + R_{n_B}},$$

which leads to

$$\frac{\delta_S^\downarrow(0) - \delta_{\min}}{\log(2)C} = R_5 + \frac{R_{n_A}R_{n_B}}{R_{n_A} + R_{n_B}},$$

the reciprocal of which reads

$$\frac{1}{R_{n_A}} + \frac{1}{R_{n_B}} = \frac{\log(2)C}{\delta_S^\downarrow(0) - \delta_{\min} - \log(2)CR_5}. \quad (45)$$

Following a similar approach for Eq. (43) and Eq. (44) and using Eq. (28) and Eq. (29) leads to

$$\frac{1}{R_{n_A}} = \frac{\log(2)C}{\delta_S^\downarrow(\infty) - \delta_{\min} - \log(2)CR_5}, \quad (46)$$

$$\frac{1}{R_{n_B}} = \frac{\log(2)C}{\delta_S^\downarrow(-\infty) - \delta_{\min} - \log(2)CR_5}. \quad (47)$$

Now, from Eq. (45), Eq. (46), and Eq. (47), it follows that

$$\frac{1}{\delta_S^\downarrow(0) - \delta_{\min} - \log(2)CR_5} = \frac{1}{\delta_S^\downarrow(\infty) - \delta_{\min} - \log(2)CR_5} + \frac{1}{\delta_S^\downarrow(-\infty) - \delta_{\min} - \log(2)CR_5},$$

which can be rewritten into a quadratic equation for $\delta_{\min} + \log(2)CR_5$. Choosing the negative solution, which ensures that $\delta_{\min} + \log(2)CR_5 \leq \delta_S^\downarrow(0)$, provides the expression for R_5 stated in Eq. (34). Plugging it into Eq. (46) and Eq. (47) gives us R_{n_A} resp. R_{n_B} according to Eq. (35) resp. Eq. (36).

Next, we focus on the parameters determined by the falling input transition case. We explain Eq. (38) by considering $A(\delta_S^\uparrow(0) - \delta_{\min}, R, R_5, C)$, which corresponds to setting $t = \delta_0 = \delta_S^\uparrow(0) - \delta_{\min}$ as defined in Eq. (25). We start out from the implicit function $I(t, \Delta) = 0$ defined in Eq. (12) for $\Delta = 0$ and $t = \delta_0$, which also causes $A = 0$ and $\sqrt{\chi} = d = a = (\alpha_1 + \alpha_2)/2R$. Recall that it is adapted to our interconnected NOR gate setting just by replacing C by C_3 given in Eq. (31). We obtain

$$e^{-\frac{\delta_0}{2RC_3}} \left(1 + \frac{\delta_0}{a}\right)^{\frac{a}{2RC_3}} = \frac{1}{2}. \quad (48)$$

Abbreviating $\alpha = \alpha_1 + \alpha_2$ and noting $a = \alpha/2R$, raising Eq. (48) to the power $2RC_3/a = C(R_5 + 2R)/a$ results in

$$e^{-\frac{\delta_0}{a}} \left(1 + \frac{\delta_0}{a}\right) = 2^{-\frac{C(R_5 + 2R)}{a}}, \quad (49)$$

which is equivalent to $(1 + \frac{2R\delta_0}{\alpha}) = 2^{-\frac{2RC(R_5 + 2R)}{\alpha}} e^{\frac{2R\delta_0}{\alpha}}$. By raising both sides to the power of $\alpha/(2R)$, we get $1 < (1 + \frac{2R\delta_0}{\alpha})^{\frac{\alpha}{2R}} = 2^{-C(R_5 + 2R)} e^{\delta_0}$. After raising it to the power $2R$ again, this can be rewritten as $(1 + \frac{\omega}{y})^y = \beta$ with $\omega =$

³Whereas there might be a way to solve it analytically, we did not find it so far.

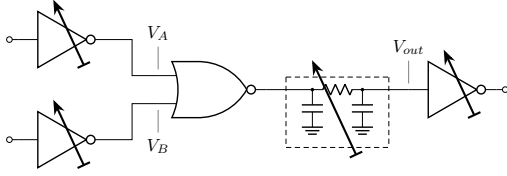


Fig. 5: Experimental setup.

$2R\delta_0 > 0$, $y = \alpha > 0$, and $\beta = e^{2R(\delta_0 - C(R_5 + 2R)\log(2))} > 1$. Substituting $z = 1 + \frac{\omega}{y} > 1$, we get $e^{\frac{\omega}{z-1}\log(z)} = \beta$, and taking the natural logarithm on both sides establishes

$$\log(z) = (z - 1)\gamma, \quad (50)$$

for $\gamma = \frac{\log(\beta)}{\omega} > 0$. We need to solve Eq. (50) for $z > 1$ so as to obtain $\alpha = y = \frac{\omega}{z}$. Exponentiation of Eq. (50) yields $ze^{-z\gamma} = e^{-\gamma}$, and multiplication by $-\gamma$ finally gives us $-z\gamma e^{-z\gamma} = -\gamma e^{-\gamma}$. We can solve this equation for $-z\gamma$ by means of the Lambert W function. Since $\gamma > 0$ and we need the solution to satisfy $z > 1$, we must take the branch W_{-1} here to compute $z = -\frac{W_{-1}(-\gamma e^{-\gamma})}{\gamma}$. Plugging in the definitions of z and γ into $y = \frac{\omega}{z}$, we obtain

$$y = -\frac{-\log(\beta)}{W_{-1}\left(-\frac{\log(\beta)}{\omega}\beta^{-\frac{1}{\omega}}\right) + \frac{\log(\beta)}{\omega}}. \quad (51)$$

Finally, replacing ω resp. β by their “generic” definitions $\omega = 2Rt$ resp. $\beta = e^{2R(t - C(R_5 + 2R)\log(2))}$ (where δ_0 is replaced by t) in Eq. (51) gives Eq. (38).

It only remains to justify Eq. (40) and Eq. (41), for which the same procedure as for Eq. (26) and Eq. (27) can be used: The same derivations as above, except that we start from the variant of Eq. (49) where a is replaced by $\frac{\alpha_1}{2R}$ resp. $\frac{\alpha_2}{2R}$ for Eq. (40) resp. Eq. (41). This finally also explains why we can determine R by (numerically) solving Eq. (39). \square

C. Experimental accuracy evaluation

In this section, we evaluate the accuracy of our interconnect-augmented model by comparing its predictions to the actual delays of an interconnected NOR gate obtained via analog simulations. More specifically, as illustrated in Fig. 5, we instantiated a NOR gate connected to an inverter, acting as its load, via a controlled wire. The inputs of the NOR gate are driven by a chain of 4 inverters acting as signal shaping gates. The chain input is stimulated by a saturated ramp with a rise/fall time of 0.1 fs, which leads to “natural” signal waveforms at the chain output.

For every setting, the following steps were performed:

- (1) Utilizing a Verilog description of our CMOS NOR gate implementation, we employed the Cadence tools Genus and Innovus (version 19.11) for placing and routing our design.
- (2) Using the extracted parasitic networks from the final layout, we performed SPICE simulations to determine $\delta^{\uparrow/\downarrow}$ for different values of Δ .
- (3) Using the measured MIS delay values $\delta_S^{\downarrow}(\infty)$, $\delta_S^{\downarrow}(0)$, $\delta_S^{\uparrow}(\infty)$ and $\delta_S^{\uparrow}(0)$, $\delta_S^{\uparrow}(-\infty)$, as well as the

measured minimal pure delay δ_{\min} determined according to the procedure described in [27] (with inputs A and B tied together) and some rough estimate⁴ of the load capacitance C , we used Theorem 3 for parametrizing our model.

- (4) Using the equations given in Corollary 1, we computed the predictions of the parametrized model for different values Δ , and compared the outcome to the measured delays.

The different settings used in the evaluation range from different implementation technologies to varying driving strengths and load capacitances to different wire lengths, wire resistances, and wire capacitances. Most of these results were obtained for a CMOS NOR gate from the 15 nm Nangate Open Cell Library featuring FreePDK15TM FinFET models [28] with a supply voltage of $V_{DD} = 0.8$ V. Qualitatively similar results have been obtained for the UMC 65 nm technology with $V_{DD} = 1.2$ V.

Overall, the accuracy of our interconnect-augmented model turned out to be very good. This is in stark contrast to the original model [21] for isolated NOR gates, where even the parametrization procedure in step (3) already failed in most scenarios considered in this paper. This confirms that adding R_5 is really instrumental for modeling interconnected gates.

A representative sample of our results will be presented in the following subsections. In all our figures, the SPICE-generated delays are depicted by the dashed red curve, whereas the delays predicted by our model are represented by the blue curve.

1) *Wire length*: Utilizing the 15nm technology, we varied the length of the wire driven by the NOR gate across the range of $l = 3$ to $l = 15$ micrometers⁵. The model parameters are given in Table IV, and the results are shown in Fig. 6. The modeling accuracy is indeed remarkable.

TABLE IV: Model parameter values for two wire lengths $l = 3 \mu\text{m}$ and $l = 15 \mu\text{m}$, for which $\delta_{\min} = 4.32$ ps and $\delta_{\min} = 5.08$ ps, respectively. The chosen load capacitance is $C = 1.2831$ fF.

Parameters for $l = 3 \mu\text{m}$		
$R_{n_A} = 2.1936$ k Ω	$R_{n_B} = 2.011$ k Ω	$R_5 = 399.41$ Ω
$R = 1.2771$ k Ω	$\alpha_1 = 1.078e - 9$ Ωs	$\alpha_2 = 0.5102e - 9$ Ωs
Parameters for $l = 15 \mu\text{m}$		
$R_{n_A} = 2.9$ k Ω	$R_{n_B} = 2.7493$ k Ω	$R_5 = 360.49$ Ω
$R = 2.0545$ k Ω	$\alpha_1 = 1.479e - 9$ Ωs	$\alpha_2 = 0.8441e - 9$ Ωs

2) *Wire resistance and capacitance*: In order to verify the ability of our model to adapt to varying parasitic networks, we artificially changed the resistances and capacitances of the extracted network for wire length $l = 15 \mu\text{m}$: in one setting, we halved all the resistor values, and in another setting, we doubled the values of all capacitors. Table V gives the model parameters and Fig. 7 shows the results, again revealing a very good match.

3) *Load capacitance*: Additionally, we explored varying the load capacitance of the 15nm NOR gate with wire lengths

⁴Our parametrization procedure can adapt to any value for C , by scaling the resistors R_{n_A} , R_{n_B} and R appropriately.

⁵Note that l actually corresponds to the parameter \$LENGTH in the command `relativePlace inv1 nor1 -relation R -xOffset $LENGTH -yOffset 0`, and thus approximately represents the length in μm , disregarding vias.

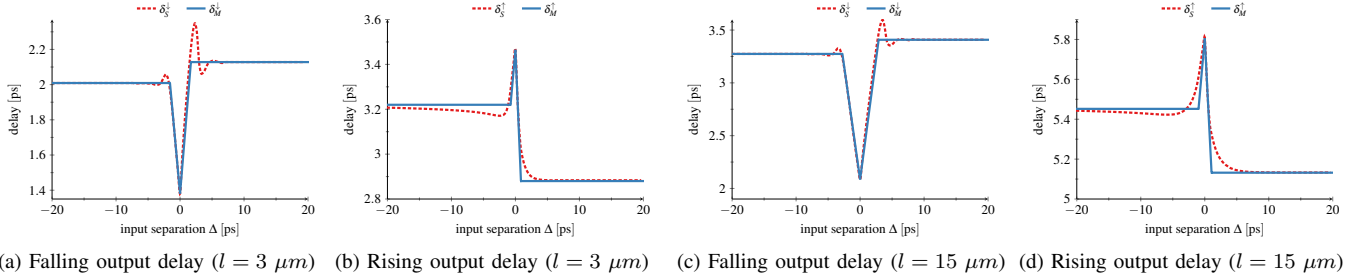


Fig. 6: SPICE-generated ($\delta_S^{\uparrow/\downarrow}(\Delta)$) and predicted ($\delta_M^{\uparrow/\downarrow}(\Delta)$) MIS delays for a 15nm technology NOR gate for different wire lengths l .

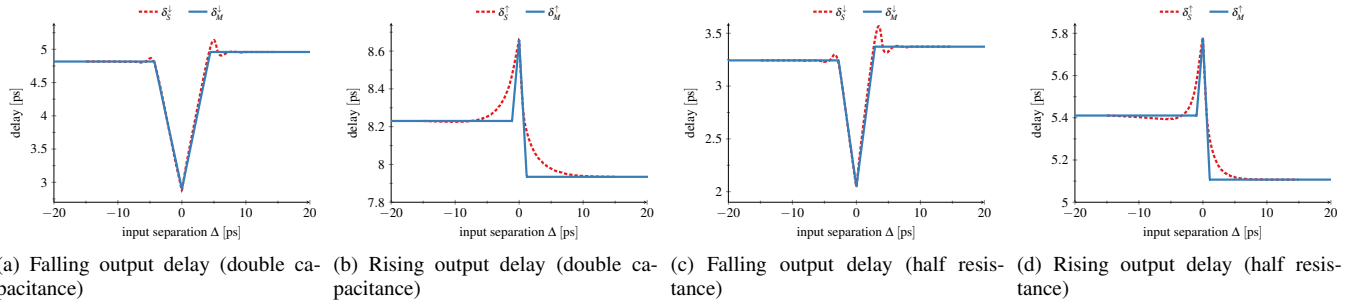


Fig. 7: SPICE-generated ($\delta_S^{\uparrow/\downarrow}(\Delta)$) and predicted ($\delta_M^{\uparrow/\downarrow}(\Delta)$) MIS delays for a 15nm technology NOR gate for wire length $l = 15 \mu\text{m}$ when the wire capacitances are doubled (two left figures) resp. the wire resistors are halved (two right figures).

TABLE V: Model parameter values for different wire resistances and capacitances, with $\delta_{min} = 0.51 \text{ ps}$ and $\delta_{min} = 0.46 \text{ ps}$ for double capacitance and half resistance. The chosen load capacitance value is $C = 1.2831 \text{ fF}$.

Parameters for doubling the capacitance		
$R_{nA} = 4.5510 \text{ k}\Omega$	$R_{nB} = 4.3896 \text{ k}\Omega$	$R_5 = 447.11 \Omega$
$R = 3.5436 \text{ k}\Omega$	$\alpha_1 = 2.215e - 9 \Omega\text{s}$	$\alpha_2 = 1.393e - 9 \Omega\text{s}$
Parameters for half the resistor values		
$R_{nA} = 2.9037 \text{ k}\Omega$	$R_{nB} = 2.7578 \text{ k}\Omega$	$R_5 = 366.26 \Omega$
$R = 2.0503 \text{ k}\Omega$	$\alpha_1 = 1.486e - 9 \Omega\text{s}$	$\alpha_2 = 0.88e - 9 \Omega\text{s}$

of $l = 3 \mu\text{m}$ and $l = 15 \mu\text{m}$, achieved by increasing the fan-out of the NOR gate acting as a load. To accomplish this, we used inverters comprising 2, 4, and 8 parallel pMOS and nMOS transistors. The outcomes of these experiments, which used the parametrization given in Table VI, are depicted in Fig. 8. Note that we had to incorporate different (increasing) values for C in each case, to match the quite different (increasing) measured delays.

TABLE VI: Model parameter values for different load capacitances.

Parameters for Fig. 8a and Fig. 8b.			
$C = 1.2831 \text{ fF}$	$\delta_{min} = 0.41 \text{ ps}$	$R_{nA} = 2.1496 \text{ k}\Omega$	$R_{nB} = 2.0068 \text{ k}\Omega$
$R_5 = 355.82 \Omega$	$R = 1.3993 \text{ k}\Omega$	$\alpha_1 = 1.075e - 9 \Omega\text{s}$	$\alpha_2 = 0.564e - 9 \Omega\text{s}$
Parameters for Fig. 8c and Fig. 8d.			
$C = 2.9775 \text{ fF}$	$\delta_{min} = 0.29 \text{ ps}$	$R_{nA} = 2.6760 \text{ k}\Omega$	$R_{nB} = 2.5921 \text{ k}\Omega$
$R_5 = 232.77 \Omega$	$R = 2.1640 \text{ k}\Omega$	$\alpha_1 = 1.273e - 9 \Omega\text{s}$	$\alpha_2 = 0.785e - 9 \Omega\text{s}$
Parameters for Fig. 8e and Fig. 8f.			
$C = 1.2831 \text{ fF}$	$\delta_{min} = 0.46 \text{ ps}$	$R_{nA} = 3.4405 \text{ k}\Omega$	$R_{nB} = 3.2801 \text{ k}\Omega$
$R_5 = 434.88 \Omega$	$R = 2.5447 \text{ k}\Omega$	$\alpha_1 = 1.697e - 9 \Omega\text{s}$	$\alpha_2 = 0.984e - 9 \Omega\text{s}$
Parameters for Fig. 8g and Fig. 8h.			
$C = 3.2831 \text{ fF}$	$\delta_{min} = 0.41 \text{ ps}$	$R_{nA} = 2.6738 \text{ k}\Omega$	$R_{nB} = 2.5997 \text{ k}\Omega$
$R_5 = 197.55 \Omega$	$R = 2.2261 \text{ k}\Omega$	$\alpha_1 = 1.138e - 9 \Omega\text{s}$	$\alpha_2 = 0.693e - 9 \Omega\text{s}$

4) *Input gate driving strength*: In two other settings, we varied the driving strength of the two input inverters in Fig. 5 that drive V_A and V_B of the 15 nm NOR gate connected to the load inverter via a wire of length $l = 15 \mu\text{m}$. More

specifically, we used both a strong input inverter (comprising four parallel pMOS and nMOS transistors) and a weak input inverter (which was simulated by letting the input inverters drive three additional NOR gates, resulting in a fan-out of four). Fig. 9 shows the outcomes for both scenarios, which have been obtained using the model parameters listed in Table VII.

TABLE VII: Model parameter values associated with different input gate driving strength.

Parameters for Fig. 9a and Fig. 9b.			
$C = 1.2831 \text{ fF}$	$\delta_{min} = 0.78 \text{ ps}$	$R_{nA} = 3.3696 \text{ k}\Omega$	$R_{nB} = 3.3344 \text{ k}\Omega$
$R_5 = 895.42 \Omega$	$R = 2.1595 \text{ k}\Omega$	$\alpha_1 = 1.634e - 9 \Omega\text{s}$	$\alpha_2 = 0.942e - 9 \Omega\text{s}$
Parameters for Fig. 9c and Fig. 9d.			
$C = 1.2831 \text{ fF}$	$\delta_{min} = 0.41 \text{ ps}$	$R_{nA} = 2.8899 \text{ k}\Omega$	$R_{nB} = 2.7053 \text{ k}\Omega$
$R_5 = 231.29 \Omega$	$R = 2.0305 \text{ k}\Omega$	$\alpha_1 = 1.526e - 9 \Omega\text{s}$	$\alpha_2 = 1.083 \Omega\text{s}$

5) *Other technologies*: To validate that our model achieves comparable modeling accuracies also in different technologies, we conducted additional simulations for a NOR gate in UMC 65 nm technology with a supply voltage of $V_{DD} = 1.2 \text{ V}$. Given the qualitative similarity of the results, we present only a very small subset in this paper: Figure 10 shows the results for two different wire lengths $l \in \{5, 25\}$, based on the parameters given in Table VIII.

TABLE VIII: Model parameter values for different wire lengths in 65 nm technology.

Parameters for Fig. 9a and Fig. 9b.			
$C = 6.2831 \text{ fF}$	$\delta_{min} = 1.76 \text{ ps}$	$R_{nA} = 6.2629 \text{ k}\Omega$	$R_{nB} = 5.8159 \text{ k}\Omega$
$R_5 = 4.089 \text{ k}\Omega$	$R = 600.66 \Omega$	$\alpha_1 = 3.483e - 9 \Omega\text{s}$	$\alpha_2 = 0.908e - 9 \Omega\text{s}$
Parameters for Fig. 9c and Fig. 9d.			
$C = 7.2831 \text{ fF}$	$\delta_{min} = 1.109 \text{ ps}$	$R_{nA} = 8.1075 \text{ k}\Omega$	$R_{nB} = 7.7869 \text{ k}\Omega$
$R_5 = 4.3430 \text{ k}\Omega$	$R = 2.065 \Omega$	$\alpha_1 = 9.687e - 9 \Omega\text{s}$	$\alpha_2 = 3.073 \Omega\text{s}$

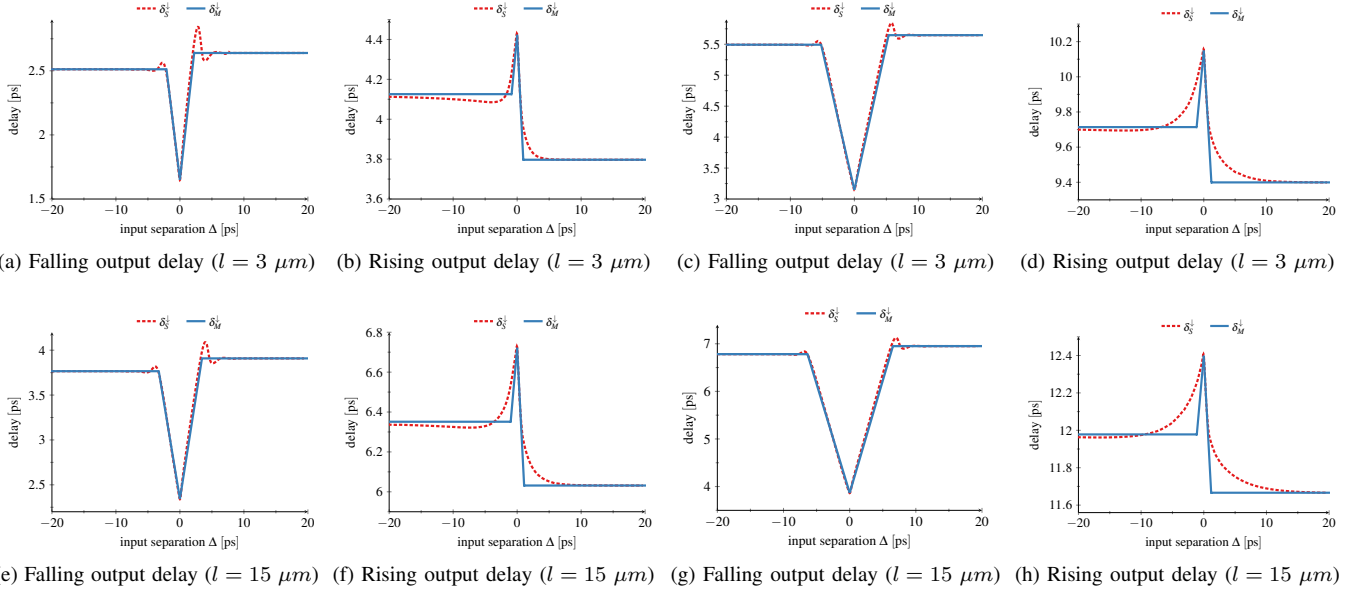


Fig. 8: SPICE-generated ($\delta_S^{\uparrow/\downarrow}(\Delta)$) and predicted ($\delta_M^{\uparrow/\downarrow}(\Delta)$) MIS delays for a 15 nm technology NOR gate driving two parallel pMOS and nMOS transistors (two left figures) and eight parallel pMOS and nMOS transistors (two right figures) for different wire lengths l .

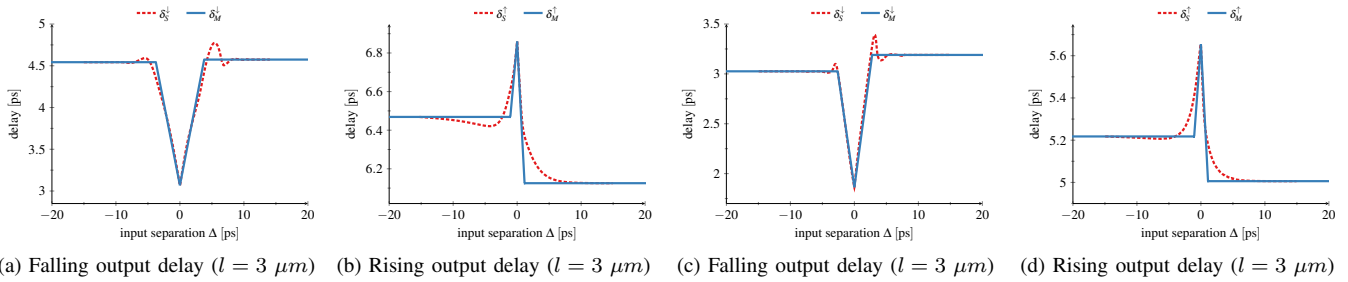


Fig. 9: SPICE-generated ($\delta_S^{\uparrow/\downarrow}(\Delta)$) and predicted ($\delta_M^{\uparrow/\downarrow}(\Delta)$) MIS delays for a 15 nm technology NOR gate for wire length $l = 15 \mu m$ with weak input drivers (two left figures) resp. strong input drivers (two right figures).

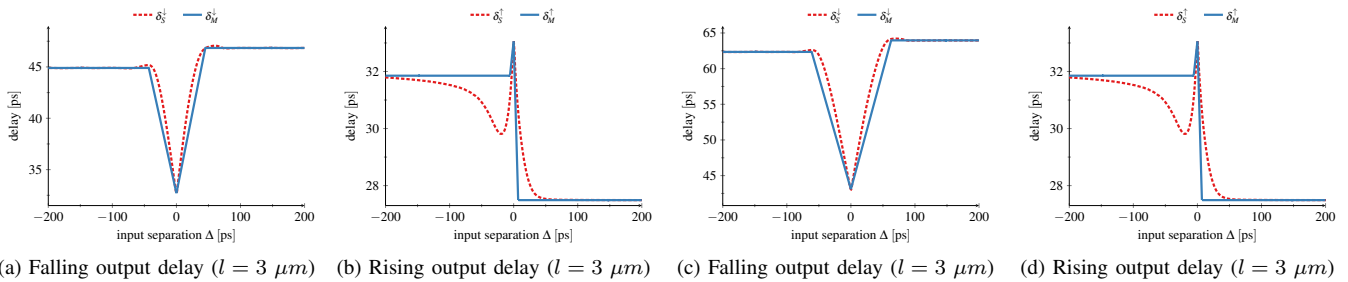


Fig. 10: SPICE-generated ($\delta_S^{\uparrow/\downarrow}(\Delta)$) and predicted ($\delta_M^{\uparrow/\downarrow}(\Delta)$) MIS delays for a 65 nm technology NOR gate with different wire length $l \in \{5 \mu m, 25 \mu m\}$.

V. AN ACCURATE HYBRID MIS DELAY MODEL FOR INTERCONNECTED MULLER C GATES

A crucial feature of a delay modeling approach like ours is broad applicability. As already explained in [21], it is easy to derive a model for (interconnected) NAND gates from a model for NOR gates by simply swapping nMOS transistors with pMOS transistors and vice versa, as well as swapping V_{DD} and GND . In this section, we will develop a thresholded

hybrid model for interconnected Muller C gates, which are core elements in asynchronous circuit designs [3]. It will turn out that adding a lumped RC model interconnect (Fig. 4c) to the thresholded hybrid model for isolated C gates introduced in [21] does not increase its coverage.

The thresholded hybrid model for isolated Muller C gates developed in [21] is based on the CMOS implementation depicted in Fig. 11a. Despite the apparent complications

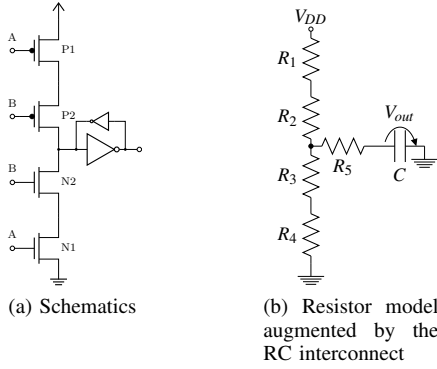


Fig. 11: CMOS C gate implementation and the resistor model equipped with the RC interconnect.

introduced by the state keeper element formed by the loop of two inverters, it turned out that one can safely disregard it in the model: the load capacitance C in the corresponding resistor model (Fig. 11b) effectively implements an ideal state keeper for V_{out} when the output is in a high-impedance state, i.e., when at least one of $P1$ and $P2$ and at least one of $N1$ and $N2$ are switched off. To accommodate the negation of the output, R_1 and R_2 were designated to correspond to the nMOS transistors $N2$ and $N1$, and R_3 and R_4 to the pMOS transistors $P1$ and $P2$. As in the case of the NOR gate, continuously varying resistors according to Eq. (1) were assumed for switching-on, and instantaneously changing resistors for switching-off, but this time for all transistors.

Applying Kirchhoff's rules to Fig. 11b results again in the first-order non-homogeneous ODE Eq. (20), albeit with

$$\frac{1}{R_g(t)} = \frac{1}{R_1(t) + R_2(t)} + \frac{1}{R_3(t) + R_4(t)}. \quad (52)$$

The approach used for solving Eq. (20) and developing the appropriate delay formulas for the interconnected NOR gate can hence be adopted also here, with the only difference that $G(t) = (I_1(t) + I_2(t))/C$, where $I_1(t) = \int_0^t \frac{ds}{R_1(s) + R_2(s)}$ and $I_2(t) = \int_0^t \frac{ds}{R_3(s) + R_4(s)}$. Table IX summarizes all possible input state transitions, the corresponding resistor mode switch timing, the relevant integrals I_1 and I_2 , and the exact or approximated value of $f(t)$.

More specifically, a detailed comparison between the transitions in Table IX and those in Table I and Table II shows that extracting the output voltage trajectories and deriving delay expressions for *both* rising and falling input transitions in C is identical to the falling input transition case of the NOR gate. The only differences are the substitution of R_p with R_n for rising input transitions, and the replacement of α_1 resp. α_2 with α_4 resp. α_3 for falling input transitions. Consequently, the delay formulas for the interconnected C gate stated in Theorem 4 are very similar to those obtained for the falling input transition case of the interconnected NOR gate.

Theorem 4 (MIS Delay functions for interconnected C gates). *For any $0 \leq |\Delta| \leq \infty$, the MIS delay functions of our model for rising and falling input transitions are respectively given*

by

$$\delta_{M,+}^{\uparrow}(\Delta) = \begin{cases} \delta_0^{\uparrow} - \frac{\alpha_1}{\alpha_1 + \alpha_2} \Delta & 0 \leq \Delta < \frac{(\alpha_1 + \alpha_2)(\delta_0^{\uparrow} - \delta_{-\infty}^{\uparrow})}{\alpha_1} \\ \delta_{-\infty}^{\uparrow} & \Delta \geq \frac{(\alpha_1 + \alpha_2)(\delta_0^{\uparrow} - \delta_{-\infty}^{\uparrow})}{\alpha_1} \end{cases} \quad (53)$$

$$\delta_{M,-}^{\uparrow}(\Delta) = \begin{cases} \delta_0^{\uparrow} - \frac{\alpha_2}{\alpha_1 + \alpha_2} |\Delta| & 0 \leq |\Delta| < \frac{(\alpha_1 + \alpha_2)(\delta_0^{\uparrow} - \delta_{-\infty}^{\uparrow})}{\alpha_2} \\ \delta_{-\infty}^{\uparrow} & |\Delta| \geq \frac{(\alpha_1 + \alpha_2)(\delta_0^{\uparrow} - \delta_{-\infty}^{\uparrow})}{\alpha_2} \end{cases} \quad (54)$$

$$\delta_{M,+}^{\downarrow}(\Delta) = \begin{cases} \delta_0^{\downarrow} - \frac{\alpha_4}{\alpha_3 + \alpha_4} \Delta & 0 \leq \Delta < \frac{(\alpha_3 + \alpha_4)(\delta_0^{\downarrow} - \delta_{-\infty}^{\downarrow})}{\alpha_4} \\ \delta_{-\infty}^{\downarrow} & \Delta \geq \frac{(\alpha_3 + \alpha_4)(\delta_0^{\downarrow} - \delta_{-\infty}^{\downarrow})}{\alpha_4} \end{cases} \quad (55)$$

$$\delta_{M,-}^{\downarrow}(\Delta) = \begin{cases} \delta_0^{\downarrow} - \frac{\alpha_3}{\alpha_3 + \alpha_4} |\Delta| & 0 \leq |\Delta| < \frac{(\alpha_3 + \alpha_4)(\delta_0^{\downarrow} - \delta_{-\infty}^{\downarrow})}{\alpha_3} \\ \delta_{-\infty}^{\downarrow} & |\Delta| \geq \frac{(\alpha_3 + \alpha_4)(\delta_0^{\downarrow} - \delta_{-\infty}^{\downarrow})}{\alpha_3} \end{cases} \quad (56)$$

where

$$\delta_0^{\uparrow} = -\frac{\alpha_1 + \alpha_2}{2R_n} \left[1 + W_{-1} \left(\frac{-1}{e \cdot 2 \frac{2R_n C (R_5 + 2R_n)}{\alpha_1 + \alpha_2}} \right) \right], \quad (57)$$

$$\delta_{-\infty}^{\uparrow} = -\frac{\alpha_2}{2R_n} \left[1 + W_{-1} \left(\frac{-1}{e \cdot 2 \frac{2R_n C (R_5 + 2R_n)}{\alpha_2}} \right) \right], \quad (58)$$

$$\delta_0^{\downarrow} = -\frac{\alpha_3 + \alpha_4}{2R_p} \left[1 + W_{-1} \left(\frac{-1}{e \cdot 2 \frac{2R_p C (R_5 + 2R_p)}{\alpha_3 + \alpha_4}} \right) \right], \quad (60)$$

$$\delta_{-\infty}^{\downarrow} = -\frac{\alpha_4}{2R_p} \left[1 + W_{-1} \left(\frac{-1}{e \cdot 2 \frac{2R_p C (R_5 + 2R_p)}{\alpha_4}} \right) \right]. \quad (62)$$

A. Model parametrization

Due to the similarity of both rising and falling input transitions in our C gate modeling to the falling input transition case of the NOR gate, it turns out that the parametrization for the C gate involves determining R_n and R_p using two functions, both of which are in the form of Eq. (38). The following Theorem 5 provides the detailed procedure.

Theorem 5 (Model parametrization for interconnect-augmented C gates). *Let $\delta_{\min} > 0$ be the pure delay and $\delta_S^{\downarrow}(-\infty)$, $\delta_S^{\downarrow}(0)$, $\delta_S^{\downarrow}(\infty)$ and $\delta_S^{\uparrow}(-\infty)$, $\delta_S^{\uparrow}(0)$, $\delta_S^{\uparrow}(\infty)$ be the extremal MIS delay values of a real interconnected C gate that shall be matched by our model. Given an arbitrary chosen value C for the load capacitance, this is accomplished by choosing the model parameters as follows: For*

$$B(t, z, C) = \frac{-(t - Cz \log(2))}{W_{-1} \left(\left(\frac{Cz \log(2)}{t} - 1 \right) e^{\frac{Cz \log(2)}{t} - 1} \right) + 1 - \frac{Cz \log(2)}{t}}, \quad (63)$$

TABLE IX: State transitions, integrals $I_1(t)$ and $I_2(t)$, and the function $U(t)$ for the C gate. $2R_p = R_{p_A} + R_{p_B}$ and $2R_n = R_{n_A} + R_{n_B}$.

Transition	t_A	t_B	R_1	R_2	R_3	R_4	$I_1(t) = \int_0^t \frac{ds}{R_1(s)+R_2(s)}$	$I_2(t) = \int_0^t \frac{ds}{R_3(s)+R_4(s)}$	$U(t) = \frac{V_{DD}}{C(R_1(t)+R_2(t))}$	$f(t) = \frac{1}{\frac{R_5}{R_5+1} + 1}$
(0,0) → (1,0)	0	−∞	on → off	on	off → on	off	0	0	0	= 1
(1,0) → (1,1)	− Δ	0	off	on → off	on	off → on	$\int_0^t (1/(\frac{\alpha_1}{s+\Delta} + \frac{\alpha_2}{s} + 2R_n)) ds$	0	$V_{DD}/(C(\frac{\alpha_1}{t+\Delta} + \frac{\alpha_2}{t} + 2R_n))$	$\approx \frac{2R_n}{R_5+2R_n}$
(0,0) → (0,1)	−∞	0	on	on → off	off	off → on	0	0	0	= 1
(0,1) → (1,1)	0	− Δ	on → off	off	off → on	on	$\int_0^t (1/(\frac{\alpha_1}{s} + \frac{\alpha_2}{s+\Delta} + 2R_n)) ds$	0	$V_{DD}/(C(\frac{\alpha_1}{t} + \frac{\alpha_2}{t+\Delta} + 2R_n))$	$\approx \frac{2R_n}{R_5+2R_n}$
(1,1) → (0,1)	0	−∞	off → on	off	on → off	on	0	0	0	= 1
(0,1) → (0,0)	− Δ	0	on	off → on	off	on → off	0	$\int_0^t (1/(\frac{\alpha_3}{s} + \frac{\alpha_4}{s+\Delta} + 2R_p)) ds$	0	$\approx \frac{2R_p}{R_5+2R_p}$
(1,1) → (1,0)	−∞	0	off	off → on	on	on → off	0	0	0	= 1
(1,0) → (0,0)	0	− Δ	off → on	on	on → off	off	0	$\int_0^t (1/(\frac{\alpha_3}{s+\Delta} + \frac{\alpha_4}{s} + 2R_p)) ds$	0	$\approx \frac{2R_p}{R_5+2R_p}$

numerically solve

$$B(\delta_S^\uparrow(0) - \delta_{\min}, x, C) - B(\delta_S^\uparrow(\infty) - \delta_{\min}, x, C) - B(\delta_S^\uparrow(-\infty) - \delta_{\min}, x, C) = 0, \quad (64)$$

$$B(\delta_S^\downarrow(0) - \delta_{\min}, y, C) - B(\delta_S^\downarrow(\infty) - \delta_{\min}, y, C) - B(\delta_S^\downarrow(-\infty) - \delta_{\min}, y, C) = 0. \quad (65)$$

for x and y , respectively. For any choice of $0 \leq R_5 < \min\{x, y\}$, let $R_n = (x - R_5)/2 > 0$ and $R_p = (y - R_5)/2 > 0$, and choose

$$\alpha_1 = 2R_n B(\delta_S^\uparrow(-\infty) - \delta_{\min}, x, C), \quad (66)$$

$$\alpha_2 = 2R_n B(\delta_S^\uparrow(\infty) - \delta_{\min}, x, C), \quad (67)$$

$$\alpha_3 = 2R_p B(\delta_S^\downarrow(-\infty) - \delta_{\min}, y, C), \quad (68)$$

$$\alpha_4 = 2R_p B(\delta_S^\downarrow(\infty) - \delta_{\min}, y, C). \quad (69)$$

Proof. The correspondence of both the rising and falling input transition case of the C gate to the falling input transition case allows us to re-use Eq. (38) for the interconnected NOR gate, i.e.,

$$A(t, R, R_5, C) = \frac{-2R(t - C(R_5 + 2R) \cdot \log(2))}{W_{-1}\left(\left(\frac{C(R_5 + 2R) \cdot \log(2)}{t} - 1\right)e^{\frac{C(R_5 + 2R) \cdot \log(2)}{t} - 1}\right) + 1 - \frac{C(R_5 + 2R) \cdot \log(2)}{t}}, \quad (70)$$

The definition of Eq. (63) ensures

$$A(t, R_n, R_5, C) = \frac{B(t, R_5 + 2R_n, C)}{2R_n}, \quad (71)$$

$$A(t, R_p, R_5, C) = \frac{B(t, R_5 + 2R_p, C)}{2R_p}. \quad (72)$$

Whereas we cannot numerically solve the analog of Eq. (39) for both functions since R_n , R_p and R_5 are unknown, we can numerically solve the equivalent equations Eq. (64) for x and Eq. (65) for y .

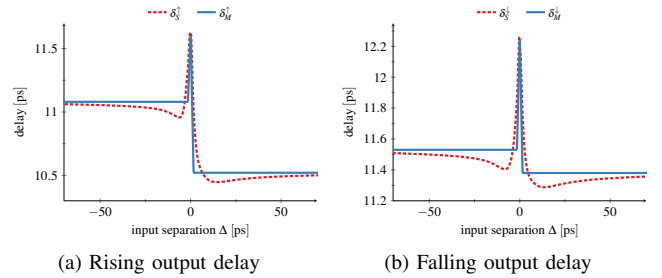
Since $x = R_5 + 2R_n$ and $y = R_5 + 2R_p$, one can choose R_5 freely within $[0, \min\{x, y\}]$. Using the resulting value of R_n resp. R_p and recalling Eq. (40) and Eq. (41) yields Eq. (66) and Eq. (67) resp. Eq. (68) and Eq. (69). \square

B. Experimental accuracy evaluation

We first consider an isolated 15nm C gate with parameters shown in Table X, with $R_5 = 0$. Fig. 12a and Fig. 12b show the results, which reveal a very good match between the SPICE-generated and predicted delays.

TABLE X: Model parameter values for the 15nm C gate with chosen value of $C = 2.6331 \text{ fF}$, $\delta_{\min} = 1.77e - 12$, and $R_5 = 0$.

$R_n = 2.1420 \text{ k}\Omega$	$\alpha_1 = 2.1472 \text{ }\Omega\text{s}$	$\alpha_2 = 1.1303 \text{ }\Omega\text{s}$
$R_p = 2.3215 \text{ k}\Omega$	$\alpha_3 = 1.5549 \text{ }\Omega\text{s}$	$\alpha_4 = 1.8403 \text{ }\Omega\text{s}$


Fig. 12: Computed ($\delta_M^{\uparrow/\downarrow}(\Delta)$) and measured ($\delta_S^{\uparrow/\downarrow}(\Delta)$) MIS delays for a 15nm technology isolated C gate.

For interconnected C gates, we showcase some results by varying the length, resistance, and capacitance of the wire. Table XI and Table XIII present the relevant parameters for different wire lengths and different resistance/capacitance values of the wire, for essentially random choices of R_5 . To demonstrate that the choice of R_5 (within the bounds stated in Theorem 5) is irrelevant for the modeling accuracy, Table XII and Table XIV provide the analogous parametrizations for the choice $R_5 = 0$.

Fig. 13 and Fig. 14 show the corresponding results, for both choices of R_5 , which again show a very good match.

TABLE XI: Model parameter values for two wire lengths $l = 3 \mu\text{m}$ and $l = 15 \mu\text{m}$, for C gates with $\delta_{\min} = 1.7 \text{ ps}$ and $\delta_{\min} = 1.77 \text{ ps}$, respectively. The chosen load capacitance values is $C = 2.6331 \text{ fF}$, the chosen value for R_5 given below is essentially random.

Parameters for $l = 3 \mu\text{m}$			
$R_n = 964.76 \text{ }\Omega$	$R_p = 1.146 \text{ k}\Omega$	$R_5 = 545.49 \text{ }\Omega$	
$\alpha_1 = 645.48e - 12 \text{ }\Omega\text{s}$	$\alpha_2 = 264.94e - 12 \text{ }\Omega\text{s}$	$\alpha_3 = 255.59e - 12 \text{ }\Omega\text{s}$	$\alpha_4 = 406.81e - 12 \text{ }\Omega\text{s}$
Parameters for $l = 15 \mu\text{m}$			
$R_n = 1.418 \text{ k}\Omega$	$R_p = 1.487 \text{ k}\Omega$	$R_5 = 801.28 \text{ }\Omega$	
$\alpha_1 = 991.49e - 12 \text{ }\Omega\text{s}$	$\alpha_2 = 396.18e - 12 \text{ }\Omega\text{s}$	$\alpha_3 = 942.30e - 12 \text{ }\Omega\text{s}$	$\alpha_4 = 1.20e - 12 \text{ }\Omega\text{s}$

TABLE XII: Model parameter values for two wire lengths $l = 3 \mu\text{m}$ and $l = 15 \mu\text{m}$, for C gates with $\delta_{\min} = 1.7 \text{ ps}$ and $\delta_{\min} = 1.77 \text{ ps}$, respectively. The chosen load capacitance values is $C = 2.6331 \text{ fF}$, and $R_5 = 0$.

Parameters for $l = 3 \mu\text{m}$			
$R_n = 1.237 \text{ k}\Omega$	$R_p = 1.419 \text{ k}\Omega$	$R_5 = 0 \text{ }\Omega$	
$\alpha_1 = 827.97e - 12 \text{ }\Omega\text{s}$	$\alpha_2 = 339.84e - 12 \text{ }\Omega\text{s}$	$\alpha_3 = 316.40e - 12 \text{ }\Omega\text{s}$	$\alpha_4 = 503.61e - 12 \text{ }\Omega\text{s}$
Parameters for $l = 15 \mu\text{m}$			
$R_n = 1.818 \text{ k}\Omega$	$R_p = 1.888 \text{ k}\Omega$	$R_5 = 0 \text{ }\Omega$	
$\alpha_1 = 1000.27e - 12 \text{ }\Omega\text{s}$	$\alpha_2 = 508.10e - 12 \text{ }\Omega\text{s}$	$\alpha_3 = 1000.19e - 12 \text{ }\Omega\text{s}$	$\alpha_4 = 1000.52e - 12 \text{ }\Omega\text{s}$

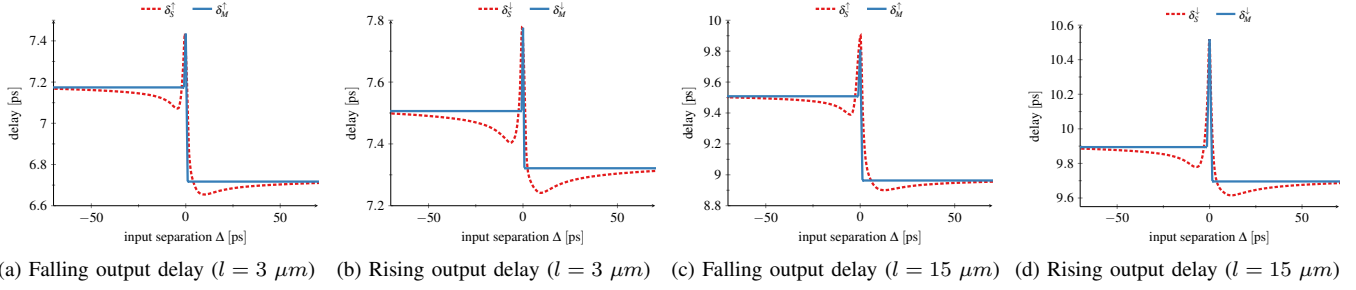


Fig. 13: SPICE-generated ($\delta_S^{\uparrow/\downarrow}(\Delta)$) and predicted ($\delta_M^{\uparrow/\downarrow}(\Delta)$) MIS delays for a 15nm technology C gate for different wire lengths l , for any feasible choice of R_5 .

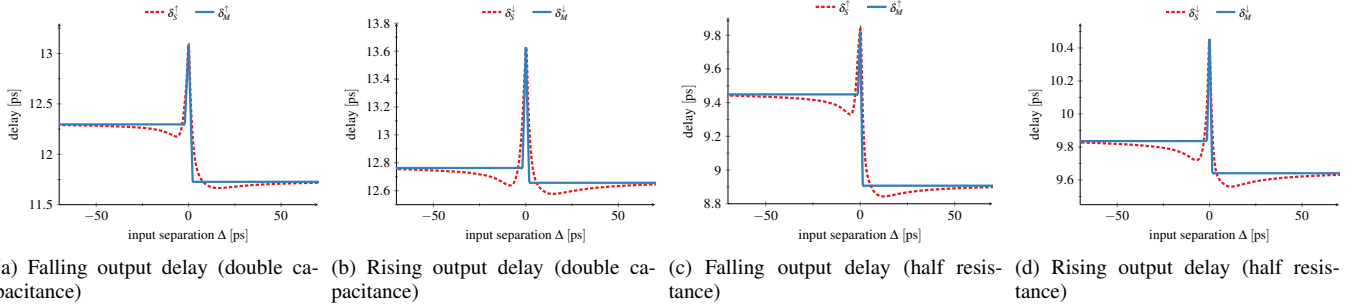


Fig. 14: SPICE-generated ($\delta_S^{\uparrow/\downarrow}(\Delta)$) and predicted ($\delta_M^{\uparrow/\downarrow}(\Delta)$) MIS delays for a 15nm technology C gate for wire length $l = 15 \mu\text{m}$ when the wire capacitances are doubled (two left figures) resp. the wire resistors are halved (two right figures), for any feasible choice of R_5 .

TABLE XIII: Model parameter values for different wire resistances and capacitances of the C gate with chosen values of $\delta_{min} = 1.3 \text{ ps}$ and $\delta_{min} = 1.74 \text{ ps}$ for double capacitance and half resistance. The chosen load capacitance values is $C = 2.6331 \text{ fF}$, the chosen value for R_5 given below is essentially random.

Parameters for doubling the capacitance			
$R_n = 1.794 \text{ k}\Omega$	$R_p = 2.060 \text{ k}\Omega$	$R_5 = 1.013 \text{ k}\Omega$	
$\alpha_1 = 2.614e - 9 \Omega\text{s}$	$\alpha_2 = 1.629e - 19 \Omega\text{s}$	$\alpha_3 = 1.728e - 9 \Omega\text{s}$	$\alpha_4 = 1.912e - 9 \Omega\text{s}$
Parameters for half the resistor values			
$R_n = 1.383 \text{ k}\Omega$	$R_p = 1.492 \text{ k}\Omega$	$R_5 = 781.49 \Omega$	
$\alpha_1 = 1.138e - 9 \Omega\text{s}$	$\alpha_2 = 0.516e - 9 \Omega\text{s}$	$\alpha_3 = 0.931e - 9 \Omega\text{s}$	$\alpha_4 = 1.184e - 9 \Omega\text{s}$

TABLE XIV: Model parameter values for different wire resistances and capacitances of the C gate with chosen values of $\delta_{min} = 1.3 \text{ ps}$ and $\delta_{min} = 1.74 \text{ ps}$ for double capacitance and half resistance. The chosen load capacitance values is $C = 2.6331 \text{ fF}$, and $R_5 = 0$.

Parameters for doubling the capacitance			
$R_n = 2.301 \text{ k}\Omega$	$R_p = 2.567 \text{ k}\Omega$	$R_5 = 0 \Omega$	
$\alpha_1 = 3.353e - 9 \Omega\text{s}$	$\alpha_2 = 2.089e - 19 \Omega\text{s}$	$\alpha_3 = 2.154e - 9 \Omega\text{s}$	$\alpha_4 = 2.383e - 9 \Omega\text{s}$
Parameters for half the resistor values			
$R_n = 1.773 \text{ k}\Omega$	$R_p = 1.882 \text{ k}\Omega$	$R_5 = 0 \Omega$	
$\alpha_1 = 1.459e - 9 \Omega\text{s}$	$\alpha_2 = 662.113e - 9 \Omega\text{s}$	$\alpha_3 = 1.176e - 9 \Omega\text{s}$	$\alpha_4 = 1.495e - 9 \Omega\text{s}$

VI. CONCLUSION

In this paper, we developed thresholded first-order hybrid delay models for interconnected multi-input gates, in particular, two-input NOR and Muller C gates, which accurately capture multi-input switching (MIS) effects. Besides analytic formulas for all MIS delays in terms of the parameters, we also provided procedures for determining the model parameters that allow our models to match the extremal MIS delays of a given real circuit. We demonstrated their high modeling accuracy by means of simulations performed in a wide range of different settings, including varying wire lengths, resis-

tances/capacitances, input driving strengths, and output load capacitances for two different CMOS technologies.

REFERENCES

- [1] *CCS Timing Library Characterization Guidelines*, Synopsis Inc., October 2016, version 3.4.
- [2] *Effective Current Source Model (ECSM) Timing and Power Specification*, Cadence Design Systems, January 2015, version 2.1.2.
- [3] A. J. Winstanley, A. Garivier, and M. R. Greenstreet, "An Event Spacing Experiment," in *Proceedings of the 8th International Symposium on Asynchronous Circuits and Systems (ASYNC)*, April 2002, pp. 47–56.
- [4] L.-C. Chen, S. K. Gupta, and M. A. Breuer, "A new gate delay model for simultaneous switching and its applications," in *Proceedings of the 38th Design Automation Conference*, 2001, pp. 289–294.
- [5] L. W. Nagel and D. Pederson, "SPICE (Simulation Program with Integrated Circuit Emphasis)," EECS Department, University of California, Berkeley, Tech. Rep. UCB/ERL M382, 1973.
- [6] F. N. Najm, "A survey of power estimation techniques in vlsi circuits," *IEEE Transactions on Very Large Scale Integration (VLSI) Systems*, vol. 2, no. 4, pp. 446–455, 1994.
- [7] S. H. Unger, "Asynchronous sequential switching circuits with unrestricted input changes," *IEEE Transaction on Computers*, vol. 20, no. 12, pp. 1437–1444, 1971.
- [8] M. Függer, T. Nowak, and U. Schmid, "Unfaithful glitch propagation in existing binary circuit models," *IEEE Transactions on Computers*, vol. 65, no. 3, pp. 964–978, 2016.
- [9] M. Függer, R. Najvirt, T. Nowak, and U. Schmid, "A faithful binary circuit model," *IEEE Transactions on Computer-Aided Design of Integrated Circuits and Systems*, vol. 39, no. 10, pp. 2784–2797, 2020.
- [10] M. Függer, J. Maier, R. Najvirt, T. Nowak, and U. Schmid, "A faithful binary circuit model with adversarial noise," in *2018 Design, Automation Test in Europe Conference Exhibition (DATE)*, March 2018, pp. 1327–1332. [Online]. Available: <https://ieeexplore.ieee.org/document/8342219/>
- [11] D. Öhlinger and U. Schmid, "A digital delay model supporting large adversarial delay variations," in *26th International Symposium on Design and Diagnostics of Electronic Circuits and Systems, DDECS 2023, Tallinn, Estonia, May 3-5, 2023*, M. Jenihhin, H. Kubátová,

- N. Metens, J. Raik, F. Ahmed, and J. Belohoubek, Eds. IEEE, 2023, pp. 111–117. [Online]. Available: <https://doi.org/10.1109/DDECS57882.2023.10139680>
- [12] A. Ferdowsi, M. Függer, T. Nowak, and U. Schmid, “Continuity of thresholded mode-switched odes and digital circuit delay models,” in *Proceedings of the 26th ACM International Conference on Hybrid Systems: Computation and Control*, ser. HSCC’23. New York, NY, USA: Association for Computing Machinery, 2023. [Online]. Available: <https://doi.org/10.1145/3575870.3587125>
- [13] D. Öhlinger, J. Maier, M. Függer, and U. Schmid, “The involution tool for accurate digital timing and power analysis,” *Integration*, vol. 76, pp. 87–98, 2021.
- [14] R. Najvirt, U. Schmid, M. Hofbauer, M. Függer, T. Nowak, and K. Schweiger, “Experimental validation of a faithful binary circuit model,” in *Proceedings of the 25th Edition on Great Lakes Symposium on VLSI*, ser. GLSVLSI ’15. New York, NY, USA: ACM, 2015, pp. 355–360. [Online]. Available: <http://doi.acm.org/10.1145/2742060.2742081>
- [15] A. R. Subramaniam, J. Roveda, and Y. Cao, “A finite-point method for efficient gate characterization under multiple input switching,” *ACM Trans. Des. Autom. Electron. Syst.*, vol. 21, no. 1, pp. 10:1–10:25, Dec. 2015. [Online]. Available: <http://doi.acm.org/10.1145/2778970>
- [16] J. Shin, J. Kim, N. Jang, E. Park, and Y. Choi, “A gate delay model considering temporal proximity of multiple input switching,” in *2009 International SoC Design Conference (ISOCC)*, Nov 2009, pp. 577–580.
- [17] V. Chandramouli and K. A. Sakallah, “Modeling the effects of temporal proximity of input transitions on gate propagation delay and transition time,” in *Proc. DAC’96*, 1996, p. 617–622. [Online]. Available: <https://doi.org/10.1145/240518.240635>
- [18] J. Sridharan and T. Chen, “Modeling multiple input switching of cmos gates in dsm technology using hdmr,” in *Proceedings of the Design Automation Test in Europe Conference*, vol. 1, March 2006, pp. 6 pp.–.
- [19] O. V. S. Shashank Ram and S. Saurabh, “Modeling multiple-input switching in timing analysis using machine learning,” *IEEE Transactions on Computer-Aided Design of Integrated Circuits and Systems*, vol. 40, no. 4, pp. 723–734, 2021.
- [20] A. Ferdowsi, J. Maier, D. Öhlinger, and U. Schmid, “A simple hybrid model for accurate delay modeling of a multi-input gate,” in *Proceedings of the 2022 Design, Automation & Test in Europe Conference & Exhibition*, 2022.
- [21] A. Ferdowsi, U. Schmid, and J. Salzmänn, “Accurate hybrid delay models for dynamic timing analysis,” in *2023 IEEE/ACM International Conference on Computer Aided Design (ICCAD)*. IEEE, 2023, pp. 1–9.
- [22] A. Ferdowsi, M. Függer, T. Nowak, U. Schmid, and M. Drmota, “Faithful dynamic timing analysis of digital circuits using continuous thresholded mode-switched odes,” *arXiv preprint arXiv:2403.03235*, 2024.
- [23] H. Shichman and D. A. Hodges, “Modeling and simulation of insulated-gate field-effect transistor switching circuits,” *IEEE Journal of Solid-State Circuits*, vol. 3, no. 3, pp. 285–289, 1968.
- [24] A. Ferdowsi, M. Függer, J. Salzmänn, and U. Schmid, “A hybrid delay model for interconnected multi-input gates,” in *2023 26th Euromicro Conference on Digital System Design (DSD)*, 2023, pp. 381–390.
- [25] N. de Bruijn, *Asymptotic methods in analysis*, 3rd ed., ser. Bibliotheca Mathematica. Netherlands: North-Holland Publishing Company, 1970.
- [26] M. R. Jan, C. Anantha, N. Borivoje *et al.*, “Digital integrated circuits: a design perspective,” *Pearson*, 2003.
- [27] J. Maier, D. Öhlinger, U. Schmid, M. Függer, and T. Nowak, “A composable glitch-aware delay model,” in *Proceedings of the 2021 on Great Lakes Symposium on VLSI*, 2021, pp. 147–154.
- [28] M. Martins, J. M. Matos, R. P. Ribas, A. Reis, G. Schlinker, L. Rech, and J. Michelsen, “Open cell library in 15nm freepdk technology,” in *Proceedings of the 2015 Symposium on International Symposium on Physical Design*, ser. ISPD ’15. New York, NY, USA: ACM, 2015, pp. 171–178. [Online]. Available: <http://doi.acm.org/10.1145/2717764.2717783>